

1 **Response to Referee #2:**

2
3 [Responses to individual comments are given here below:](#)

4
5 [Overall the authors have done a goodly amount of change to the paper as the marked revision shows. The
6 paper is well written and with current figures that are both legible and concise for the paper. The revision
7 now includes discussion in various places of the jump/drift with IASI that was not in the original draft.
8 They have also re-done their trend analyses in accordance to this jump/drift in IASI.]

9 [We thank the referee for her/his appreciation for the changes made in the manuscript in order to address all](#)
10 [the two referees' comments.](#)

11
12 [In the revision the authors have added discussion of a downward “jump” in tropospheric ozone
13 measurements around September 2010 for IASI which they mention causes an artificial overall downward
14 trend or drift of about -2.8 DU/decade in the NH. This is new to the revision which mentions this jump
15 several times including the Conclusions section as possibly affecting the calculated trends. In an effort to
16 account for this jump the authors have modified their regression trend model by including two different
17 constants in the regression for the two separate time periods, before and after September 2010. An argument
18 is made that the jump-related drift of -2.8 DU does not explain the larger negative trends in summer of ~-5
19 DU/decade measured by IASI.]

20 The authors state that the reason for the downward jump in tropospheric ozone from IASI is not clear. The
21 reference list includes Keppens et al. and Boynard et al. papers that discuss a detected negative drift in IASI
22 tropospheric ozone. Both are related papers using IASI and are in preparation/under review for this same
23 issue; the two papers are mentioned specifically in the revision in regards to the drift/jump in IASI ozone.
24 The revision states that Boynard et al. (this issue) describes the IASI drift as being caused largely by a
25 downward discontinuity “jump” in the IASI data around September 2010. An earlier paper published by
26 Boynard et al. (2016) shows in their Figure 15 evidence of this jump and a persistent downward drift/trend
27 in IASI tropospheric ozone relative to ozonesondes in both the NH and SH extra-tropics. The downward
28 drift (including jump) for IASI tropospheric ozone relative to the ozonesondes indicated by Boynard et al.
29 (2016) was never discussed in their 2016 paper. The current revision references the Boynard and Keppens
30 papers that are under review for this same special issue regarding the IASI jump/drift.]

31 [A discontinuity was not clearly enough demonstrated in the paper of Boynard et al. \(2016\). Furthermore,](#)
32 [that paper reports the validation of the previous FORLI-O₃ product \(FORLI-v20140922\), while Boynard et](#)
33 [al. \(under review, this issue\) validates the last FORLI-O₃ product \(FORLI-v20151009\) which is the one](#)
34 [used in this manuscript and his companion paper \(Wespes et al., 2017\). As a consequence, only the results](#)
35 [reported in Boynard et al \(under review, this issue\) should be considered for the present O₃ trend analysis.](#)

36
37 [The authors state that tropospheric ozone for IASI has one piece of information that corresponds to ground-
38 to-300 hPa. The authors define this as middle-low troposphere (MLT) ozone. They mention that the upper
39 level 300 hPa tends to minimize influence from stratospheric ozone in the retrievals. The revision still states
40 that the significant negative trends in the SH are hard to explain, and mention that stratospheric ozone
41 influence may be a large reason for this band structure of negative MLT trends throughout the SH year-
42 round. There will be questions from readers regarding the very nature of IASI nadir retrievals in resolving

43 tropospheric ozone, especially how much tailing influence from ozone above 300 hPa (including
44 stratosphere) there is in the MLT measurements, especially in the extra-tropics.]

45 In a previous paper (Wespes et al., 2016), we have specifically quantified the stratospheric contributions
46 into the ground-300 hPa O₃ columns as function of the latitudes and the periods. Values from that study
47 have already been referenced here precisely to discuss critically the possible impact of the stratosphere in
48 the tropospheric O₃ trends. We don't see how to improve on this without duplicating this earlier paper.

49

50 [Papers listed in my first review describing zero or positive trends measured in extra-tropical tropospheric
51 ozone are not included in the revision. There are several reasons stated for not referencing them in the
52 revision such as issues of MLT versus UT or differences in the vertical resolution of the measurements.
53 The author's response is that including reference to these is beyond the scope of the present paper. The
54 Petetin et al. (2016) paper (the diurnal cycle paper) that I mentioned in my first review used
55 MOZAIC+IAGOS aircraft measurements over Frankfurt and showed statistically significant increases in
56 ozone throughout the troposphere from ground to 300 hPa (i.e., MLT). Regarding the TOAR, another basic
57 issue for the satellite measurements including IASI is their short records for doing trend analyses and that
58 their time periods are generally quite different.]

59 We have indeed carefully looked at the paper of Petetin et al. (2016) which is of high relevance. However,
60 considering the recent decline observed in the anthropogenic O₃ precursors in the N.H. (since 2010-2011),
61 the results presented in their Figures 5 and S6-9 are not comparable with ours. They show "relative
62 differences of O₃ mixing ratio between two periods" (1994–2003 and 2004–2012) over Frankfurt only and,
63 hence, they are not representative of the period analyzed here on global scale. For this reason, we have
64 preferred to reference the TOAR-climate report that gives an overview of O₃ trends in the troposphere that
65 have been reported from independent existing datasets including MOZAIC and IAGOS.

66

67 Moreover, we would like to stress that significant efforts have been devoted in order to disentangle trend
68 from other dynamical effects by applying a dedicated MLR model to the IASI data and that it has been
69 shown achievable even from a relatively short period of measurements (Wespes et al., 2016). While other
70 methods are also valuable, we feel that a proper comparison can only be made against studies that have
71 used similar MLR. In that respect, we now provide in the revised manuscript additional discussion based
72 on the results of Leventidou et al., (under review), Heue et al. (2016) and Ebojie et al. (2016) which have
73 applied MLR to the data from UV sounders. From these papers, one can easily see the challenge in
74 homogenizing independent datasets and reaching consensus in determining tropospheric O₃ trends.
75 Nevertheless, significant negative trends are interestingly found at the global scale (~-4 to -8 DU/dec;
76 Ebojie et al., 2016) and in the tropics over the Oceanic regions (~ -1 to -2.5 DU/dec; Leventidou et al.,
77 under review) while significant positive trends are observed over Africa (Leventidou et al., under review).
78 These results are comparable with those reported in our manuscript, despite the different studied periods
79 (1995-2015 in Leventidou et al. and 2003-2011 in Ebojie et al., 2016). These papers have been added in the
80 revised manuscript.

81

82 In order not to oversell the results, we have also made clearer in the revised manuscript (abstract, section
83 4.3 and conclusion) that, at this stage, no consensus in terms of O₃ trends can be easily reached in the
84 troposphere from the available measurements (UV or IR satellites, O₃ sondes, aircrafts, ground-based
85 measurements,...) for the reasons already mentioned in the manuscript (time-varying instrumental biases,

86 differences in the methodology used for calculating trends, in the measurement period, in the upper
87 boundary of the O₃ columns, in the retrieval algorithm, in the spatio-temporal sampling, in the vertical
88 sensitivity of the instrument,...).

89

90 [There appears to be some questions regarding the IASI MLT ozone measurements themselves for
91 evaluating trends. The drift for IASI tropospheric ozone is a bit disturbing as it is rather large and not
92 explainable from either the current study or those of Keppens et al. or Boynard et al. that are related IASI
93 papers also in review in this same issue. The negative trends throughout much of the NH and SH for IASI
94 MLT ozone appear to be in contradiction to zero or positive trends measured from other independent data
95 sources (aircraft, ozonesonde, satellite), albeit of differing (usually longer) time records and not specifically
96 calculated for ground-to-300hPa as IASI. The authors attribute negative trends in the NH as possibly due
97 to reductions in emissions in recent years, particularly over N. America and Europe. The authors state that
98 the negative trends in the SH are hard to explain, but possibly of stratospheric origin.]

99 See our responses to the two previous comments about reconciling trend with previous studies and the
100 stratospheric contribution into the S.H. trends.

101

102 We acknowledge that the origin of the artificial drift is still unclear and under investigation at present.
103 However, we feel that the inclusion of a second constant in the MLR model is a pretty robust way to deal
104 with this issue and, hence, that the jump should not interfere with the trends. The fact that this correction
105 did not change the broad results gives somewhat more confidence in the retrieved O₃ trend.

106

107 [Given over 9 years of measurements from IASI for detecting decadal changes in global tropospheric ozone
108 (main theme of the paper), it would seem important to compare decadal changes in IASI MLT ozone
109 directly with decadal changes in other independent data products in the paper such as station ozonesondes
110 or IAGOS aircraft ozone. This paper is going to raise some doubts with readers as to the IASI trend results
111 given the current unknowns with the data. There is really not enough 1-1 comparison evidence presented
112 from other independent measurements to test validity of the IASI trend results.]

113 We certainly agree that such a 1-1 comparison would be of great interest. However it is definitively not
114 straightforward as it would deserve setting careful criteria on co-locations and involve a detailed
115 investigation of the respective vertical sensitivities. Moreover, differences in spatio-temporal samplings
116 should be also investigated. Attempts have been made to apply a MLR model on the same O₃ sondes dataset
117 (smoothed by the IASI averaging kernels) as the one used for the validation in Boynard et al. (this issue).
118 Unfortunately, the regression residual errors were found too large to retrieve significant trend or dynamical
119 covariates because of the weak temporal sampling of the dataset. We feel and we would like the reviewer
120 and the editor to agree that such a 1-1 comparison is outside the scope of this paper, which again, exploits
121 the global coverage of IASI to extract relevant trends.

122

123 We also would like to stress that the validation of FORLI-O₃ in Boynard et al. (this issue) with O₃ sondes
124 highlights a jump but not a persistent downward drift, as it has been confirmed by calculating the drift
125 separately over the periods before or after the jump (cfr our responses to previous comments to referees #1
126 and #2).

127

128 Finally, we would like to notify the reviewer on the fact that such an evaluation of the different IASI-O₃
129 products against O₃ sondes and daily IAGOS commercial aircraft profiles is being initiated by the IASI data
130 providers (ULB/LATMOS, LA and LISA) in collaboration with the IAGOS data providers and the TOAR-
131 climate leaders (A. Gaudel and O. Cooper).

132
133
134
135
136
137
138
139
140
141
142
143
144
145
146
147
148
149
150
151
152
153
154
155
156
157
158
159
160
161
162
163
164
165
166
167

168 **List of relevant changes made in the manuscript:**

169

170 **Abstract:**

- 171 - **L. 23-26:** “Despite that no consensus in terms of tropospheric O₃ trends is currently
172 reached from the available independent datasets (UV or IR satellites, O₃ sondes, aircrafts,
173 ground-based measurements...) for the reasons that are discussed in the text, this finding
174 is consistent with... ”

175

176 **Section 4.1:**

- 177 - **L. 236-272:** “On the contrary, the tropical Pacific region exhibits significant negative
178 trends that are similar to those reported from UV sounders in Ebojie et al. (2016) and in
179 Leventidou et al. (in review) over previous periods, while Heue et al. (2016) mainly reports
180 significant positive trend over that region.”
- 181 - **L. 285-286:** “Significant positive trends over South-East Asia have also been reported from
182 UV sounders over previous periods (e.g. Ebojie et al., 2016).”
- 183 - **L. 303-304:** “Significant negative change in tropospheric O₃ over these regions were also
184 reported in Ebojie et al. (2016).”

185

186 **Section 4.3:**

- 187 - **L. 425 - 428:** “If reconciling the trend biases between the datasets by applying the vertical
188 sensitivity of each measurement type to a common platform, as proposed in the TOAR-
189 climate assessment report is beyond the scope of this study and if, at this stage, there is no
190 consensus in determining tropospheric O₃ trends, the improvement in using a MLR instead
191 of a SLR model ...”

192

193 **Conclusions:**

- 194 - **L. 589-594 :** “Currently, no consensus in terms of O₃ trends in the troposphere is reached
195 from the available measurements (UV or IR satellites, O₃ sondes, aircrafts, ground-based
196 measurements,...) for several reasons (time-varying instrumental biases, differences in the
197 methodology used for calculating trends, in the measurement period, in the upper boundary
198 of the O₃ columns, in the retrieval algorithm, in the spatio-temporal sampling, in the
199 vertical sensitivity of the instrument,...) (Section 4.3; the TOAR-climate report – Gaudel
200 et al., in review). However, determination, with IASI ...”

201

202 **References:**

- 203 - Ebojie, F., Burrows, J. P., Gebhardt, C., Ladstätter-Weissenmayer, A., von Savigny, C.,
204 Rozanov, A., Weber, M., and Bovensmann, H.: Global tropospheric ozone variations from
205 2003 to 2011 as seen by SCIAMACHY, Atmos. Chem. Phys., 16, 417-436,
206 doi:10.5194/acp-16-417-2016, 2016.

- 207 - Heue, K.-P., Coldewey-Egbers, M., Delcloo, A., Lerot, C., Loyola, D., Valks, P., and van
208 Roozendael, M.: Trends of tropical tropospheric ozone from 20 years of European satellite
209 measurements and perspectives for the Sentinel-5 Precursor, *Atmos. Meas. Tech.*, 9, 5037-
210 5051, doi:10.5194/amt-9-5037-2016, 2016.
- 211 - Leventidou, E., Weber, M., Eichmann, K.-U., and Burrows, J. P.: Harmonisation and trends
212 of 20-years tropical tropospheric ozone data, *Atmos. Chem. Phys. Discuss.*,
213 <https://doi.org/10.5194/acp-2017-815>, in review, 2017.

214
215
216
217
218
219
220
221
222
223
224
225
226
227
228
229
230
231
232
233
234
235
236
237
238
239
240
241
242
243
244
245
246

247 **Decrease in tropospheric O₃ levels of the Northern Hemisphere observed by IASI**

248

249 Catherine Wespes¹, Daniel Hurtmans¹, Cathy Clerbaux^{1,2}, Anne Boynard² and Pierre-François
250 Coheur¹

251 ¹Spectroscopie de l'Atmosphère, Service de Chimie Quantique et Photophysique, Faculté des
252 Sciences, Université Libre de Bruxelles (ULB), Bruxelles, Belgique

253 ²LATMOS/IPSL, UPMC Univ. Paris 06 Sorbonne Universités, UVSQ, CNRS, Paris, France

254

255

256 **Abstract**

257 In this study, we describe the recent changes in the tropospheric ozone (O₃) columns measured by
258 the Infrared Atmospheric Sounding Interferometer (IASI) onboard the Metop satellite during the
259 first 9 years of the IASI operation (January 2008 to May 2017). Using appropriate multivariate
260 regression methods, we discriminate significant linear trends from other sources of O₃ variations
261 captured by IASI. The geographical patterns of the adjusted O₃ trends are provided and discussed
262 on the global scale. Given the large contribution of the natural variability in comparison with that
263 of the trend (25-85% vs 15- 50%, respectively) to the total O₃ variations, we estimate that
264 additional years of IASI measurements are generally required to detect the estimated O₃ trends
265 with a high precision. Globally, additional 6 months to 6 years of measurements, depending on the
266 regions and the seasons, are needed to detect a trend of |5| DU/decade. An exception is interestingly
267 found during summer at mid-high latitudes of the North Hemisphere (N.H.; ~ 40°N-75°N) where
268 the large absolute fitted trend values (~|0.5| DU/yr on average) combined with the small model
269 residuals (~10%) allow the detection of a band-like pattern of significant negative trends. Despite
270 that no consensus in terms of tropospheric O₃ trends is currently reached from the available
271 independent datasets (UV or IR satellites, O₃ sondes, aircrafts, ground-based measurements,...)
272 for the reasons that are discussed in the text, This finding is consistent with the reported decrease
273 in O₃ precursor emissions in recent years, especially in Europe and US. The influence of
274 continental pollution on that latitudinal band is further investigated and supported by the analysis
275 of the O₃-CO relationship (in terms of correlation coefficient, regression slope and covariance)
276 that we found to be the strongest at northern mid-latitudes in summer.

277

278 **1 Introduction**

279

280 O₃ plays a key role throughout the whole troposphere where it is produced by the photochemical
281 oxidation of carbon monoxide (CO), non-methane volatile organic compounds (NMVOCs) and
282 methane (CH₄) in the presence of nitrogen oxides (NO_x) (e.g. Logan et al., 1981). O₃ sources in
283 the troposphere are the in situ photochemical production from anthropogenic and natural
284 precursors, and the downwards transport of stratospheric O₃. Being a strong pollutant, a major
285 reactive species and an important greenhouse gas in the upper troposphere, O₃ is of highest interest

286 for air quality, atmospheric chemistry and radiative forcing studies. Thanks to its long lifetime
287 (several weeks) relatively to transport timescales in the free troposphere (Fusco and Logan, 2003),
288 O₃ also contributes to large-scale transport of pollution far from source regions with further
289 impacts on global air quality (e.g. Stohl et al., 2002; Parrish et al., 2012) and climate. Monitoring
290 and understanding the time evolution of tropospheric O₃ at a global scale is, therefore, crucial to
291 apprehend future climate changes. Nevertheless, a series of limitations make O₃ trends particularly
292 challenging to retrieve and to interpret.

293
294 Since the 1980s, while the O₃ precursors anthropogenic emissions have increased and shifted
295 equatorward in the developing countries (Zhang et al., 2016), extensive campaigns and routine in
296 situ and remote measurements at specific urban and rural sites have provided long-term but sparse
297 datasets of tropospheric O₃ (e.g. Cooper et al., 2014 and references therein). Ultraviolet and Visible
298 (UV/VIS) atmospheric sounders onboard satellites provide tropospheric O₃ measurements with a
299 much wider coverage, but they result either from indirect methods (e.g. Fishman et al., 2005) or
300 from direct retrievals which are limited by coarse vertical resolution (Liu et al., 2010). All these
301 datasets also suffer from a lack of homogeneity in terms of measurement methods (instrument and
302 algorithm) and spatio-temporal samplings (e.g. Doughty et al., 2011; [Heue et al., 2016](#); [Leventidou
303 et al., in review](#)). Those limitations, in addition to the large natural inter-annual variability (IAV)
304 and decadal variations in tropospheric O₃ levels (due to large-scale dynamical modes of O₃
305 variations and to changes in stratospheric O₃, in stratosphere-troposphere exchanges, in precursor
306 emissions and in their geographical patterns), introduce strong biases in trends determined from
307 independent studies and datasets (e.g. Zbinden et al., 2006; Thouret et al., 2006; Logan et al.,
308 2012 ; Parrish et al., 2012 and references therein). As a consequence, determining accurate trends
309 requires a long period of high density and homogeneous measurements (e.g. Payne et al., 2017).

310
311 Such long-term datasets are now becoming obtainable with the new generation of nadir-looking
312 and polar-orbiting instruments measuring in the thermal infrared region. In particular, about one
313 decade of O₃ profile measurements, with a good sensitivity in the troposphere independently from
314 the layers above, is now available from the IASI (Infrared Atmospheric Sounding Interferometer)
315 sounder aboard the European Metop platforms, allowing to monitor regional and global variations
316 in tropospheric O₃ levels (e.g. Dufour et al., 2012; Safieddine et al., 2013; Wespes et al., 2016).

317
318 In this study, we examine the tropospheric O₃ changes behind the natural IAV as measured by
319 IASI over January 2008-May 2017. To that end, we use the approach described in Wespes et al.
320 (2017), which relies on a multi-linear regression (MLR) procedure, for accurately differentiating
321 trends from other sources of O₃ variations; the latter being robustly identified and quantified in
322 that companion study. In Section 2, we briefly review the IASI mission and the tropospheric O₃
323 product, and we shortly describe the multivariate models (annual or seasonal) that we use for fitting
324 the daily O₃ time series. In Section 3, after verifying the performance of the MLR models over the
325 available IASI dataset, we evaluate the feasibility to capture and retrieve significant trend

326 parameters, apart from natural O₃ dependencies, by performing trend sensitivity studies. In Section
327 4, we present and discuss the global distributions of the O₃ trends estimated from IASI in the
328 troposphere. The focus is given in summer over and downwind anthropogenic polluted areas of
329 the N.H. where the possibility to infer significant trends from the first ~9 years of available IASI
330 measurements is demonstrated. Finally, the O₃-CO correlations, enhancement ratios and
331 covariance are examined for characterizing the origin of the air masses in regions of positive and
332 negative trends.

333

334 **2 IASI O₃ measurements and multivariate regression**

335

336 The IASI instrument is a nadir-viewing Fourier transform spectrometer that records the thermal
337 infrared emission of the Earth-atmosphere system between 645 and 2760 cm⁻¹ from the polar Sun-
338 synchronous orbiting meteorological Metop series of satellites. Metop-A and -B have been
339 successively launched in October 2006 and September 2012. The third and last launch is planned
340 in 2018 with Metop-C to ensure homogeneous long-term IASI measurements. The measurements
341 are taken every 50 km along the track of the satellite at nadir and over a swath of 2200 km across
342 track, with a field of view of four simultaneous footprints of 12 km at nadir, which provides global
343 coverage of the Earth twice a day (at 9:30 AM and PM mean local solar time). The instrument
344 presents a good spectral resolution and a low radiometric noise, which allows the retrieval of
345 numerous gas-phase species in the troposphere (e.g. Clerbaux et al., 2009, and references therein;
346 Hilton et al., 2012; Clarisse et al., 2011).

347

348 In this paper, we use the FORLI-O₃ profiles (Fast Optimal Retrievals on Layers for IASI
349 processing chain set up at ULB; v20151001) retrieved from the IASI-A (aboard Metop-A) daytime
350 measurements (defined with a solar zenith angle to the sun < 80°) which are characterized by a
351 good spectral fit (determined here by quality flags on biased or sloped residuals, suspect averaging
352 kernels, maximum number of iteration exceeded,...) and which correspond to clear or almost-clear
353 scenes (a filter based on a fractional cloud cover below 13% has been applied; cfr Clerbaux et al.,
354 2009; Hurtmans et al., 2012). These profiles are characterized by a good vertical sensitivity in the
355 troposphere and the stratosphere (e.g. Wespes et al., 2017). The FORLI algorithm relies on a fast
356 radiative transfer and retrieval methodology based on the Optimal Estimation Method (Rodgers,
357 2000) and is fully described in Hurtmans et al. (2012). The FORLI-O₃ profiles, which are retrieved
358 at 40 constant vertical layers from surface up to 40 km and an additional 40-60 km one, have
359 already undergone thorough characterization and validation exercises (e.g. Anton et al., 2011;
360 Dufour et al., 2012; Gazeaux et al., 2012; Hurtmans et al., 2012; Parrington et al., 2012; Pommier
361 et al., 2012; Scannell et al., 2012; Oetjen et al., 2014; Boynard et al., 2016; Wespes et al., 2016;
362 Keppens et al. 2017; Boynard et al., 2017). They demonstrated a good degree of accuracy, of
363 precision and of vertical sensitivity with no instrumental drift, to capture the large-scale dynamical
364 modes of O₃ variability in the troposphere independently from the layers above (Wespes et al.,
365 2017), with the possibility to further differentiate long-term O₃ changes in the troposphere (Wespes

366 et al., 2016). Note, however, that a drift in the N.H. MLT O₃ over the whole IASI dataset is reported
367 in Keppens et al. (this issue) and Boynard et al. (this issue) from comparison with O₃ sondes. This
368 drift (~2.8DU/dec in the N.H.) is shown in Boynard et al. (this issue) to result from a discontinuity
369 (“jump” as called in Boynard et al., this issue) in September 2010 in the IASI O₃ time series, for
370 reasons that are unclear at present. Furthermore, the drift strongly decreases (<|1| DU/dec on
371 average) after the “jump” and it becomes even non-significant for most of the stations (significant
372 positive drift is also found for some stations) over the periods before or after the jump, separately.
373

374 For the purpose of this work, we focus on a tropospheric column ranging from ground to 300 hPa
375 (called MLT – Middle-Low Troposphere – in this study) that includes the altitude of maximum
376 sensitivity of IASI in the troposphere (usually between 4 and 8 km altitude), which limits as much
377 as possible the influences of the stratospheric O₃ and that was shown in Wespes et al. (2017) to
378 exhibit independent deseasonalized anomalies/dynamical processes from those in the stratospheric
379 layers. The stratospheric contribution into the tropospheric O₃ columns have been previously
380 estimated in Wespes et al. (2016) as ranging between 30% and 65% depending on the region and
381 the season with the smallest contribution as well as the largest sensitivity in the northern mid-
382 latitudes in spring-summer where the O₃ variations, hence, mainly originate from the troposphere.
383 We use almost the same MLR model (in its annual or its seasonal formulation) as the one
384 developed in the companion paper (see Eq.1 and 2; Section 2.2 in Wespes et al., 2017), which
385 includes a series of geophysical variables in addition to a linear trend (LT) term. In order to take
386 account of the observed “jump” properly, we modified the previously used MLR model so that the
387 constant term is split into two components covering the periods before and after the September
388 2010 “jump”, separately. The MLR which is performed using an iterative stepwise backward
389 elimination approach to retain the most relevant explanatory variables (called “proxies”) at the end
390 of the iterations (e.g. Mäder et al., 2007) is applied on the daily IASI O₃ time series. The main
391 selected proxies used to account for the natural variations in O₃ are namely the QBO (Quasi-
392 Biennial Oscillation), the NAO (North Atlantic Oscillation) and the ENSO (El Niño–Southern
393 Oscillation) (cfr Table 1 in Wespes et al. (2017) for the exhaustive list of the used proxies). Their
394 associated standard errors are estimated from the covariance matrix of the regression coefficients
395 and are corrected to take into account the uncertainty due to the autocorrelation of the noise
396 residual (see Eq. 3 in Wespes et al. (2016)). The common rule that the regression coefficients are
397 significant if they are greater in magnitude than 2 times their standard errors is applied (95%
398 confidence limits defined by 2σ level). The MLR model was found to give a good representation
399 of the IASI O₃ records in the troposphere over 2008-2016, allowing us to identify/quantify the
400 main O₃ drivers with marked regional differences in the regression coefficients. Time-lags of 2
401 and 4 months for ENSO are also included hereafter in the MLR model to account for a large but
402 delayed impact of ENSO on mid- and high latitudes O₃ variations far from the Equatorial Pacific
403 where the ENSO signal originates (Wespes et al., 2017).

404

405 **3 Regression performance and sensitivity to trend**

406

407 In this section, we first verify the performance of the MLR models (annual and seasonal; in terms
408 of residual errors and variation explained by the model) to globally reproduce the time evolution
409 of O₃ records over the entire studied period (January 2008 – May 2017). Based on this, we then
410 investigate the statistical relevance for a trend study from IASI in the troposphere by examining
411 the sensitivity of the pair IASI-MLR to the retrieved LT term.

412

413 Figure 1 presents the seasonal distributions of tropospheric O₃ measured by IASI averaged over
414 January 2008 – May 2017 (left panels), along with the root-mean-squared error of the seasonal
415 regression fit (*RMSE*, in DU; middle panels) and the contribution of the fitted seasonal model into

416 the IASI O₃ time series (in %; right panels), calculated as $\frac{\sigma(O_3^{\text{Fitted_model}}(t))}{\sigma(O_3(t))}$ where σ is the standard

417 deviation relative to the regression models and to the IASI O₃ time series. These two statistical
418 parameters help to evaluate how well the fitted model explains the variability in the IASI O₃
419 observations. The seasonal patterns of O₃ measurements are close to those reported in Wespes et
420 al. (2017) for a shorter period (see Section 2.1 and 3.1 in Wespes et al. (2017) for a detailed
421 description of the distributions) and they clearly show, for instance, high O₃ values over the highly
422 populated areas of Asia in summer. The distributions from Fig.1 show that the model reproduces
423 between 35% and 90% of the daily O₃ variation captured by IASI and that the residual errors varies
424 between 0.01 DU and 5 DU (i.e. the *RMSE* relative to the IASI O₃ time series are of ~15% on
425 global average and vary between 10% in the N.H. in summer and 30% in specific tropical regions).
426 On an annual basis (data not shown), the model explains a large fraction of the variation in the
427 IASI O₃ dataset (from ~45% to ~85%) and the *RMSE* are lower than 4.5 DU everywhere (~3 DU
428 on the global average). The relative *RMSE* is less than 1% in almost all situations indicating the
429 absence of bias.

430

431 The seasonal distributions of the contribution to the total variation in the MLT from the adjusted
432 harmonic terms and explanatory variables, which account for the “natural” variability, and from
433 the LT term are shown in Fig. 2 (left and right panels, respectively). The grey areas in the LT
434 panels refer to the LT terms rejected by the stepwise backward elimination process. The crosses
435 indicate that the trend estimate in the grid cell is non-significant in the 95% confidence limits (2 σ
436 level) when accounting for the autocorrelation in the noise residual at the end of the elimination
437 procedure. While the large influence of the seasonal variations and of the main drivers - namely
438 ENSO, NAO and QBO - on the IASI O₃ records has been clearly attested in Wespes et al. (2017),
439 we demonstrate in Fig.2 that the LT also contributes considerably to the O₃ variations detected by
440 IASI in the troposphere. The LT contribution generally ranges from 15% to 50%, with the largest
441 values (~30-50%) being observed at mid-high latitudes in the S.H. (30°S-70°S) and in the N.H.
442 (~45°N-70°N) in summer. In the S.H., they are associated with the smallest tropospheric O₃
443 columns (Fig.1; left panels) and the smallest natural contributions (<25%; left panels), while in the

444 N.H. summer, they interestingly correspond to large MLT O₃ columns, large natural contributions
445 (~50-60%) and the smallest *RMSE* (<12 % or <3 DU). From the annual regression model, the
446 natural variation and the trend contribute respectively for 30-85% and up to 40% to the total
447 variation in the MLT.

448 In Fig.3, we further investigate the robustness of the estimated trends by performing sensitivity
449 tests in regions of significant trend contributions (e.g. in the N.H. mid-latitudes in summer; cfr
450 Fig.2). The ~9-year time series of IASI O₃ daily averages (dark blue) along with the results from
451 the seasonal regression model with and without the LT term included in the model (light blue and
452 orange lines, respectively) are represented in the top row panel for one specific location (Fig.3a
453 and b; highlighted by a blue circle in the JJA panel in Fig.4). The second row panel provides the
454 deseasonalised IASI (dark blue line) and fitted time series (calculated by subtracting the adjusted
455 seasonal cycle from the time series) resulting from the adjustment with and without the LT term
456 included in the MLR model (light blue and orange lines, respectively). The differences between
457 the fitted models with and without LT are shown in the third rows (pink lines). They match fairly
458 well the adjusted trend over the IASI period (3^d row panel, grey lines; the trend and the *RMSE*
459 values are also indicated) and the adjustment without LT leads to larger residuals (e.g.
460 *RMSE_{JJA_wo_LT}*=3.37 DU vs. *RMSE_{JJA_with_LT}*=3.21 DU in summer). This result demonstrates the
461 possibility to capture trend information from ~9 years of IASI-MLR with only some compensation
462 effects by the other explanatory variables, contrary to what was observed when considering a
463 shorter period of measurements or a lesser temporal sampling (i.e. monthly dataset; e.g. Wespes
464 et al., 2016). It is also worth to mention that the O₃ changes calculated over the whole IASI dataset
465 in summer are larger than the *RMSE* of the model residuals (increase of 5.39±1.86 DU vs *RMSE*
466 of 3.21 DU), underlying the statistical relevance of trend estimates.

467 The robustness of the adjusted trend is verified at the global scale in Fig.4 which represents the
468 seasonal distributions of the relative differences in the *RMSE* with and without the LT included in
469 the MLR model, calculated as $[(RMSE_{wo_LT} - RMSE_{with_LT})/RMSE_{with_LT} \times 100]$ (in %). An
470 increase in the *RMSE* when excluding LT from the MLR is observed almost everywhere in regions
471 of significant trend contributions (Fig.2), especially in mid-high latitudes of the S.H. and of the
472 N.H. in summer where it reaches 10%. This result indicates that adjusting LT improves the
473 performance of the model and, hence, that a trend signal is well captured by IASI at a regional
474 scale in the troposphere. From the annual model, the increase in the *RMSE* only reaches 5% at
475 mid-high latitudes of the S.H. (data not shown). In regions of weak or non-significant trend
476 contribution (see crosses in Fig.2), no improvement is logically found.

477

478 **4 O₃ trend over 2008-2017**

479 **4.1 Annual and seasonal trends**

480

481 The annual and the seasonal distributions of the fitted LT terms which are retained in the annual
482 and the seasonal MLR models by the stepwise elimination procedure are respectively represented
483 in Fig. 5 (a) and (b) (in DU/yr). Generally, the mid-high latitudes of both hemispheres and, more
484 particularly, the N.H. mid-latitudes in summer reveal significant negative trends, while the tropics
485 are mainly characterized by non-significant or weak significant trends. Even if trends in emissions
486 have already been able to qualitatively explain measured tropospheric O₃ trends over specific
487 regions, the magnitude and the trend estimates considerably vary between independent
488 measurement datasets (e.g. Cooper et al., 2014; the TOAR report—~~Tropospheric Ozone~~
489 ~~Assessment Report: Present day distribution and trends of tropospheric ozone relevant to climate~~
490 ~~and global atmospheric chemistry model evaluation, Lead Authors: A. Gaudel and O.R. Cooper—~~
491 coordinated by the International Global Atmospheric Chemistry Project and available on
492 <http://www.igacproject.org/activities/TOAR> – ~~Gaudel et al., in review and submitted to Elementa~~;
493 and references therein) for the reasons discussed in Section 1 and they are not
494 reproduced/explained by model simulations (e.g. Jonson et al., 2006; Cooper et al., 2010; Logan
495 et al., 2012; Wilson et al., 2012; Hess et al., 2013; and references therein). As a result,
496 comparing/reconciling the adjusted trends with independent measurements, even on a qualitative
497 basis, remains difficult. Nevertheless, several of the statistically significant features observed in
498 Fig.5 show, interestingly, qualitative consistency with respect to recent published findings:

499
500 - The S.H. tropical region extending from the Amazon to tropical eastern Indian Ocean
501 seems to indicate a general increase with, for example, a DJF trend of $\sim 0.23 \pm 0.18$ DU/yr
502 (i.e. 2.09 ± 1.70 DU over the IASI measurement period), despite the large IAV in the MLT
503 which characterizes the tropics and which likely explains the high frequency of non-
504 significant trends. Enhanced O₃ levels over that region have already been analysed for
505 previous periods (e.g. Logan et al., 1985, 1986; Fishman et al., 1991; Moxim et al., 2000;
506 Thompson et al., 2000, 2007; Sauvage et al., 2006, 2007; [Heue et al., 2016](#); [Ebojje et al.,](#)
507 [2016](#); Archibald et al., 2017; [Leventidou et al., in review](#)). For instance, the large O₃
508 enhancement of $\sim 0.36 \pm 0.25$ DU/yr (i.e. 3.3 ± 2.3 DU over the whole IASI period) stretching
509 from southern Africa to Australia over the north-east of Madagascar during the austral
510 winter-spring likely originates from large IAV in the subtropical jet-related stratosphere–
511 troposphere exchanges which have been found to primarily contribute to the tropospheric
512 O₃ trends over that region (Liu et al., 2016; 2017). Nevertheless, this finding should be
513 mitigated by the fact that the trend value in the S.H. tropics is of the same magnitude as the
514 *RMSE* of the regression residuals (~ 2 - 4.5 DU; see Fig.1).

515 On the contrary, the tropical Pacific region exhibits significant negative trends that are
516 similar to those reported from UV sounders in Ebojje et al. (2016) and in Leventidou et al.
517 (in review) over previous periods, while Heue et al. (2016) mainly reports significant
518 positive trend over that region.

519

- 520 - The trends over the South-East Asia are mostly non-significant and vary by season. In
521 spring-summer, some grid cells in India, in mainland China and eastwards downwind
522 China exhibit significant positive trends reaching ~ 0.45 DU/yr (i.e. ~ 4.2 DU over the IASI
523 measurement period). This tends to indicate that the tropospheric O_3 increases which have
524 been shown to mainly result from a strong positive trend in the Asian emissions over the
525 past decades (e.g. Zhao et al., 2013; Cooper et al., 2014; Zhang et al., 2016; Cohen et al.,
526 2017; Tarasick et al., 2017; and references therein) but also from a substantial change in
527 the stratospheric contribution (Verstraeten et al., 2015) persists through 2008-2017 despite
528 the recent decrease in O_3 precursor emissions recorded in China after 2011 (e.g. Duncan et
529 al., 2016; Krotkov et al., 2016; Miyazaki et al., 2017; Van der A et al. 2017). This would
530 indicate that this decrease is probably too recent/weak to recover the 2008 O_3 levels over
531 the entire region. Significant positive trends over South-East Asia have also been reported
532 from UV sounders over previous periods (e.g. Ebojje et al., 2016). Note, however, that this
533 finding has to be taken carefully given the large model residuals ($RMSE$ of $\sim 2-4$ DU; cfr
534 Section 3, Fig.1) over that region. Finally, the large uncertainty in trend estimates over the
535 South-East Asia might reflect the large IAV in the biomass-burning emissions and
536 lightning NO_x sources, in addition to the recent changes in emissions.
- 537
- 538 - The mid- and high latitudes of the S.H. show clear patterns of negative trends, all over the
539 year and in a more pronounced manner during winter-spring, with larger amplitudes than
540 those of the $RMSE$ values ($\sim -0.33 \pm 0.14$ DU/yr on average in the $35^\circ S-65^\circ S$ band; i.e. a
541 trend amplitude of $\sim |3.1| \pm 1.3$ DU over the studied period vs a $RMSE$ value of ~ 2.5 DU).
542 These significant negative trends in the S.H. are hard to explain but, considering the
543 stratospheric contribution into the tropospheric columns (natural and artificial due to the
544 limited IASI vertical sensitivity) in the mid-high latitudes of the S.H. ($\sim 40-60\%$; see
545 supplementary materials in Wespes et al., 2016) and the negative significant trends
546 previously reported from IASI in the UTLS/low stratosphere in the $30^\circ S-50^\circ S$ band, they
547 could be in line with those derived by Zeng et al. (2017) in the UTLS for a clean rural site
548 of the S.H. (Lauder, New Zealand), which mainly originate from increasing tropopause
549 height and O_3 depleting substances. Significant negative change in tropospheric O_3 over
550 these regions were also reported in Ebojje et al. (2016).
- 551
- 552 - In the N.H., a band-like pattern of negative trends is observed in the $40^\circ N-75^\circ N$ latitudes
553 covering Europe and North America, especially during summer. Averaged annual trend of
554 -0.31 ± 0.17 DU/yr and summer trend of -0.47 ± 0.22 DU/yr (i.e. -2.87 ± 1.57 DU and -
555 4.36 ± 2.02 DU, respectively, from January 2008 to May 2017) are estimated in that
556 latitudinal band. These trend values are significantly larger than the $RMSE$ of the MLR
557 model (< 3.5 DU in JJA; cfr Section 3, Fig.1). Interestingly, both the annual and summer
558 trends are amplified relative to the ones calculated in the mid-latitudes of the N.H. over the
559 2008-2013 period of IASI measurements (-0.19 ± 0.05 DU/yr and -0.30 ± 0.10 DU/yr for the

560 annual and the summer trends, respectively, calculated in the 30°N-50°N band; see Wespes
 561 et al. (2016)). This finding is line with previous studies which point out a possible leveling
 562 off of tropospheric O₃ in summer due to the decline of anthropogenic O₃ precursor
 563 emissions observed since 2010-2011 in North America, in Western Europe and also in
 564 some regions of China (e.g. Cooper et al., 2010; 2012; Logan et al., 2012; Parrish et al.,
 565 2012; Oltmans et al., 2013; Simon et al., 2015; [Ebojie et al., 2016](#); Archibald et al., 2017;
 566 Miyazaki et al., 2017). It even goes a step further by suggesting a possible decrease in the
 567 tropospheric O₃ levels. Archibald et al. (2017) recently reported a net decrease of ~5% in
 568 the global anthropogenic NO_x emissions in the 30°N-90°N latitude band, which is
 569 consistent with the annual significant negative trend of -0.27±0.15 DU/yr for O₃ estimated
 570 from IASI in that band. We should also note that, even if these latitudes are characterized
 571 by the lowest stratospheric contribution (~30-45%; see supplementary materials in Wespes
 572 et al., 2016), it might partly mask/attenuate the variability in the tropospheric O₃ levels.

573 574 4.2 Expected year for trend detection

575
 576 In this section, we further verify that it is indeed possible to infer, from the studied IASI period,
 577 the significant negative trend derived in the 40°N-75°N band in summer (~|0.5| DU/yr on average,
 578 see Section 4.1) by determining the expected year from which such a trend amplitude would be
 579 detectable at a global scale. This is achieved by estimating the minimum duration (with probability
 580 0.90) of the IASI O₃ measurements that would be required to detect a trend of a specified
 581 magnitude, and its 95% confidence level, following the formalism developed in Tiao et al. (1990)
 582 and in Weatherhead et al. (1998):

$$583 \quad N^* \approx \left[\frac{3.3 \cdot \sigma_\varepsilon}{|\tau_{yr}|} \cdot \sqrt{\frac{1+\Phi}{1-\Phi}} \right]^{2/3} \quad \text{Eq (1)}$$

$$584 \quad CL_{N^*} = [N^* \cdot e^{-B}; N^* \cdot e^{+B}] \quad \text{Eq (2)}$$

585 Where N^* is the number of the required years, σ_ε is the standard deviation of the autoregressive
 586 noise residual ε_t , τ_{yr} is the magnitude of the trend per year, Φ is the lag-1 autocorrelation of the
 587 noise. The magnitude of the variation and of the autocorrelation in the noise residuals are taken
 588 into account for a better precision on the trend estimate. Given that large variance (σ_ε^2) and large
 589 positive autocorrelation Φ of the noise induce small signal-to-noise ratio and long trend-like
 590 segments in the dataset, respectively, these two parameters increase the number of years that would
 591 be required for detecting a specified trend. CL_{N^*} is the 95% confidence limits which is not
 592 symmetric around N^* and depends on B , an estimated uncertainty factor calculated as

593 $\frac{4}{3\sqrt{D}} \sqrt{\frac{1+\Phi}{1-\Phi}}$, with D the number of days in the IASI datasets, which accounts for the uncertainty

594 in Φ (the uncertainty in σ_ε being negligible given that only a few years of data are needed to
595 estimate it; cfr Weatherhead et al. (1998)). As a result, based on the available IASI-A and proxies
596 datasets and assuming that the MLR model used in this study is accurate, we estimate, in Fig. 6 (a)
597 and (b), the expected year when an O₃ trend amplitude of $|5|$ DU per decade (i.e. $\tau_{yr} = |0.5|$ DU/yr
598 which corresponds to the averaged absolute value of the fitted negative trends in the N.H. summer;
599 see Fig.5b) is detectable, and its associated maximal confidence limit, respectively. The results in
600 Fig. 6 clearly demonstrates the possibility to infer, from the available IASI dataset, such significant
601 trends in the mid- and high latitudes of the N.H. in summer and fall (trend detectable from ~2016-
602 2017 with an uncertainty of ~6-9 months; cfr Fig.6b). On the contrary, the tropical regions and the
603 N.H. in winter-spring would require additional ~ 6 months to 6 years of measurements to detect
604 an amplitude of $|0.5|$ DU/yr (trend significant only from ~ 2017 – 2023 or after depending on the
605 location and the season). Note also that the strongest negative trends (up to -0.85 DU/yr, i.e. $\tau_{yr} =$
606 $|0.85|$ DU/yr, see Fig.5b) observed in specific regions of the N.H. mid-latitudes would only require
607 ~6 years of IASI measurements for being detected. The mid- and high latitudes of the S.H. would
608 require the shortest period of IASI measurement for detecting a specified trend, with only ~7 years
609 \pm 6 months of IASI measurements to detect a $|0.5|$ DU/yr trend (trend detectable from ~2015). That
610 band-like pattern in the S.H. corresponds to the region with the weakest IAV and contribution from
611 large-scale dynamical modes of variability in the IASI MLT columns (see Section 3, Fig.1 and 2),
612 which translates into small σ_ε^2 and Φ . Note however that an additional few months of IASI data
613 are required to confirm the smaller negative trend of ~-0.35 DU/yr measured on average in the
614 S.H. (see Fig.5; a period ~9 years \pm 6 months being necessary to detect a trend amplitude of $|3.5|$
615 DU/dec). Given that large σ_ε means large noise residual in the IASI data, the regions of short or
616 long required measurement period coincide, as expected, well with the small or high $RMSE$ values
617 of the regression residuals (see Section 3, Fig. 1).

618
619 The regions of the longest measurement periods required in the tropics for a trend detection (up to
620 ~16 years of IASI data) correspond to known patterns of widespread high O₃: (a) above intense
621 biomass burnings in Amazonia and eastwards across tropical Atlantic (Logan et al., 1986; Fishman
622 et al., 1991; Moxim et al., 2000; Thompson et al., 2000, 2007; Sauvage et al., 2007), (b) eastwards
623 Africa across the South Indian Ocean which is subject to large variations in the stratospheric
624 influences during the winter-spring austral period (JJA-SON) (Liu et al., 2016; 2017), (c)
625 Eastwards Africa across the North Indian Ocean to India likely due to large lightning NO_x
626 emissions above central Africa during the wet season associated with the northeastward jet
627 conducting a so-called “O₃ river” (Tocquer et al., 2015) and (d) above regions of positive ENSO
628 “chemical” effect in Equatorial Asia/Australia and eastwards above northern and southern tropical
629 regions (Wespes et al., 2016) explained by reduced rainfalls and biomass fires during El Niño

630 conditions (e.g. Worden et al., 2013). In fact, most of these patterns (a, b and d) are closely
631 connected with strong El- Niño events which extend the duration of the dry season and cause
632 severe droughts, producing intense biomass burning emissions, for instance, over South America
633 (e.g. Chen et al., 2011; Lewis et al., 2011) and South Asia/Australia (e.g. Oman et al., 2013; Valks
634 et al., 2014; Ziemke et al., 2015), and which alter the tropospheric circulation by increasing the
635 transport of stratospheric O₃ into the troposphere (e.g. Voulgarakis et al., 2011; Neu et al., 2014)
636 and the transport of biomass burning air masses to the Indian Ocean (Zhang et al., 2012). In
637 summary, these large-scale indirect ENSO-related variations in tropospheric O₃ and the lightning
638 NO_x impact on O₃, which are not accounted for in the MLR by specific representative proxies, are
639 misrepresented in the regression models. They induce large noise residuals, i.e. large σ_ϵ , and,
640 hence, extends the time period needed to detect a trend of any given magnitude.

641
642 Figure 6, finally, suggests that a long duration is also required, especially in summer, above and
643 east of China to quantify the anthropogenic impact on the local changes in the MLT: additional
644 3 ± 1.5 years or 5 ± 1.5 years for a given $|5|$ or $|3.5|$ DU/dec trend are respectively calculated. This
645 result could be explained by large perturbations in the MLT columns induced by recent decreases
646 after decades of almost constant increases in surface emissions in China (e.g. Cohen et al., 2017;
647 Miyazaki et al., 2017).

648 649 **4.3 Multi-linear vs single linear model**

650
651 Even if MLR have already been used for extracting trends in stratospheric and total O₃ columns
652 (e.g. Mäder et al., 2007; Frossard et al., 2013; Rieder et al., 2013; Knibbe et al., 2014), single linear
653 regressions (SLR) without discriminating the natural (chemical and dynamical) factors describing
654 the O₃ variability are still commonly used (e.g. Cooper et al., 2014; the TOAR-climate report –
655 ~~Gaudel et al., in review Tropospheric Ozone Assessment Report: Present day distribution and~~
656 ~~trends of tropospheric ozone relevant to climate and global atmospheric chemistry model~~
657 ~~evaluation, Lead Authors: A. Gaudel and O.R. Cooper – submitted to Elementa;~~ and references
658 therein). They are, however, suspected to contribute to trend biases retrieved between independent
659 measurements. In addition to the time-varying instrumental biases, trend biases can also be related
660 to differences in the spatial and the temporal samplings (e.g. Doughty et al., 2011; Saunio et al.,
661 2012; Lin et al., 2015), in the measurement period, in the upper boundary of the O₃ columns, in
662 the algorithm and in the vertical sensitivity of the measurements. The latter artificially alters the
663 characteristics of the sounded layer by contaminations from the above and the below layers leading
664 to a mixing of the trend but also of the natural characteristics originating from these different layers
665 (e.g. troposphere and stratosphere). The differences in the studied period, in the tropopause
666 definition and in the spatio-temporal sampling might also imply differences in the natural influence
667 on the measured O₃ variations. While the impact of the natural contribution is taken into account
668 in the MLR model, it might introduce an additional bias in the trend determined from SLR, making

669 further challenging to compare trends estimated from a series of inhomogeneous independent
670 measurements. Substantial effort in homogenizing independent tropospheric O₃ column (TOCs)
671 datasets have been performed in the TOAR-climate assessment report (Gaudel et al., [in](#)
672 [review submitted to Elementa](#)), but large SLR trend biases remain between the TOAR datasets, in
673 particular, between the satellite datasets where the lack of homogeneity in terms of tropopause
674 calculation (same tropopause definition but different temperature profiles are used), of instrument
675 vertical sensitivities and of spatial sampling has been specifically pointed as possible causes for
676 the trend divergence.

677

678 ~~If R~~reconciling the trend biases between the datasets by applying the vertical sensitivity of each
679 measurement type to a common platform, as proposed in the TOAR-climate assessment report is
680 beyond the scope of this study; and if, at this stage, there is no consensus in determining
681 tropospheric O₃ trends, ~~but~~ the improvement in using a MLR instead of a SLR model for
682 determining more accurate/realistic trends is explored here by comparing the seasonal distributions
683 of the trends estimated from MLR (see Fig. 5 (b) in Section 4.1.) and from SLR (presented in
684 Fig.7). Note that the constant term in the SLR is split into two components (covering the periods
685 before and after the September 2010 “jump”) to take account of the observed “jump” (see Section
686 2). The highest differences in the fitted trends derived from the two methods are found in the
687 tropics and in some regions of the mid-latitudes of the N.H. They likely result from overlaps
688 between the LT term and other covariates. For instance, the regions with high significant SLR
689 trends (~0.3-0.6 DU/yr over the tropical western and middle Pacific) during the period extending
690 from September to May match the regions with strong El Niño/Southern Oscillation influence (cfr
691 Fig. 8 and 12 in Wespes et al., 2016). On the contrary, the MLR model lends generally weak
692 significant negative or non-significant trends in the Pacific Niño region during that period and it
693 would even need additional ~3 to 4 years of IASI measurements for detecting the fitted SLR trends
694 (see Section above). The effect of ENSO in overestimating the fitted SLR trend is further illustrated
695 on Fig. 8 which represents the time series of O₃ observed by IASI and adjusted by the annual MLR
696 model (top row) along with the deseasonalized times series (middle row) and the fitted SLR and
697 MLR trends (bottom row). The fitted signal of the ENSO proxy from the MLR regression
698 (calculated as $x_j X_{norm,j}$ following Wespes et al. (2017)) is also represented (bottom row). That
699 example clearly shows that the ENSO influence is considerably compensated by the adjustment of
700 the linear trend in the SLR regression (annual trend of -0.48 ± 0.06 DU/yr from SLR vs -0.23 ± 0.16
701 DU/yr from MLR for that example). Finally, differences between the SLR and the MLR models
702 are also observed in the region with strong positive NAO influence over the Icelandic/Arctic region
703 during MAM (see Wespes et al. (2016) for a description of the NAO-related O₃ changes). On the
704 contrary, the sub-tropical S.H. exhibit similar seasonal patterns of negative trends from both the
705 SLR and the MLR. It results from the weak natural IAV and contributions in tropospheric O₃ above
706 that region (see Section 3, Fig. 1 and 2), which, hence, limits the compensation effects.

707

708 In summary, despite the fact that considering a long period of measurements is usually
709 recommended in SLR study to overcome the dynamical cycles and, hence, to help in
710 discriminating their influences from trends, we show that, considering that some dynamics have
711 irregular or no particular periodicity (e.g. NAO, ENSO), it is not accurate enough. Furthermore,
712 accurate satellite measurements of tropospheric O₃ at a global scale are quite recent, limiting the
713 period of available and comparable datasets (e.g. Payne et al., 2017). As a consequence, we support
714 here that using a reliable multivariate regression model based on geophysical parameters and
715 adapted for each specific sounded layer is a robust method for differentiating a “true” trend from
716 any other sources of variability and, hence, that it should help in resolving trend differences
717 between independent datasets.

718

719 **4.4 Continental influence**

720

721 In this section, we use the capabilities of IASI to simultaneously measure O₃ and CO in order (1)
722 to differentiate tropospheric and stratospheric air masses, (2) to identify the regions influenced by
723 the continental export/intercontinental transport of O₃ pollution and (3) to evaluate that continental
724 influence on tropospheric O₃ trends as observed by IASI. Similar tracer correlations between CO
725 and O₃ have already been used to give insight into the photochemical O₃ enhancement in air
726 pollution transport (e.g. Parrish et al., 1993; Bertschi et al., 2005). However, there are only a few
727 studies using global satellite data for this purpose (Zhang et al., 2006; Voulgarakis et al., 2010;
728 Kim et al., 2013) and the analysis of the O₃-CO relationship for better understanding the origin of
729 O₃ trends in the troposphere has, to the best of our knowledge, never been explored.

730

731 Fig.9a and 9b show the seasonal patterns of the O₃-CO correlations (referred as R_{O₃-CO}) and of the
732 dO_3/dCO regression slopes calculated in the troposphere (from the surface to 300 hPa) over the
733 studied IASI period (January 2008 – May 2017). The dO_3/dCO regression slopes, which represent
734 the so-called O₃-CO enhancement ratio, is used to evaluate the photochemical O₃ production in
735 continental outflow regions. The R_{O₃-CO} and the dO_3/dCO distributions are similar and clearly
736 show regional and seasonal differences in the strength of the O₃-CO relationships. The patterns of
737 positive and negative correlations allows to discriminate the outflow regions characterized by
738 photochemical O₃ production from precursors (including CO) or CO destruction (both identified
739 by positive R_{O₃-CO}) from the regions characterized by O₃ loss (chemical destruction or surface
740 deposition) or by strong stratospheric contaminations (both identified by negative R_{O₃-CO}).
741 Negative R_{O₃-CO} and dO_3/dCO are measured at high latitudes of both hemispheres all over the year,
742 but more specifically at high latitudes of the S.H. in summer-fall (with R_{O₃-CO} < -0.25 on averages
743 in DJF and MMA). Given that high latitudes experience more O₃ destruction than the low latitudes
744 due to a lack of sunlight, the negative correlations for the high latitude regions might also reflect
745 air masses originating from/characterizing the stratosphere due to natural intrusion or to artificial
746 mixing with the troposphere introduced by the limited vertical sensitivity of IASI in the highest
747 latitudes (stratospheric contribution varying between ~40% and 65%; see supplementary materials

748 in Wespes et al., 2016). These processes are likely at the origin of the band-like pattern of negative
749 trends in the S.H. discussed in Sections 3 and 4.1. Negative R_{O_3-CO} and dO_3/dCO are also found
750 above the Caribbean, the Arabic Peninsula and the North Indian Ocean in JJA/SON and the South
751 Atlantic in DJF. They are in line with Kim et al. (2013) and they likely reflect the influence of
752 lightning NO_x which produce O_3 but also OH oxidizing CO (e.g. Sauvage et al., 2007; Labrador
753 et al., 2004).

754
755 Strong positive correlations are identified in both R_{O_3-CO} and dO_3/dCO patterns over the tropical
756 regions and for mid-latitudes of both Hemispheres during the peak of photochemistry in summer.
757 Maxima ($R_{O_3-CO} > 0.8$ and $dO_3/dCO > 0.5$) are detected in continental pollution outflow regions in
758 the N.H., especially downwind South-East Asia and over the South Africa/Amazonia/South
759 Atlantic region. These O_3 -CO correlation patterns from IASI are fully consistent with those
760 measured by TES (Zhang et al., 2006; 2008; Voulgarakis et al., 2010) and by OMI/AIRS (Kim et
761 al., 2013), which have been interpreted with global CTM's as originating from Asian pollution
762 influence and from combustion sources including biomass burning, respectively. The high positive
763 R_{O_3-CO} found in JJA at mid-latitudes of the N.H. are detected in a lesser extent in DJF reflecting
764 the decreasing photochemistry. It is also worth pointing out in Fig. 9 the clear hemispheric
765 differences in the R_{O_3-CO} and dO_3/dCO values at mid-high latitudes and, more particularly, the shift
766 of positive R_{O_3-CO} and dO_3/dCO towards higher latitudes of the N.H. during summer (e.g. $R_{O_3-CO} =$
767 0.24 in summer vs 0.038 in spring in the $35^\circ N - 55^\circ N$ band). As a consequence, these results suggest
768 that the band-like pattern of negative trends measured by IASI in summer might substantially
769 reflect the continental pollution influence and, hence, that it could result from the decline of
770 anthropogenic O_3 precursor emissions. Nevertheless, interpreting O_3 -CO correlations in the free
771 troposphere, especially in photochemically aged pollution plumes far from the emission sources
772 towards the highest latitudes, remains complicated by the mixing of the continental combustion
773 outflow with stratospheric air masses, in addition to the background dynamic and photochemistry
774 (e.g. Liang et al., 2007).

775
776 Finally, we also provide in Fig.9c the seasonal patterns of O_3 -CO covariances (COV_{O_3-CO}). They
777 confirm the band-like pattern of the weak natural variation captured in the S.H. mid-latitudes (see
778 Sections 3 and 4.1) and help identifying the region downwind East China, the northern mid-
779 latitudes outflow region and the South tropical region as the ones with the highest pollution
780 variability, in addition to the strongest O_3 -CO correlations. To conclude, the particularly strong
781 positive O_3 -CO relationship in terms of R_{O_3-CO} , dO_3/dCO and COV_{O_3-CO} measured over and
782 downwind North-East India/East China in summer in comparison with the ones measured
783 downwind East US and over Europe indicate that South-East Asia experiences the most of the
784 intense pollution episodes of the N.H. with the largest O_3 -CO variability ($COV_{O_3-CO} > 40 \times 10^{33}$
785 $mol^2.cm^{-4}$) and the largest O_3 enhancement ($dO_3/dCO > 0.5$) over the last decade. The strong O_3 -
786 CO relationship in that region is associated with the significant increase that is detected in the IASI

787 O₃ levels downwind East of Asia (see Section 4.1) despite the net decrease in O₃ precursor
788 emissions recorded in China after 2011 (e.g. Cohen et al., 2017; Miyazaki et al., 2017).

789

790 **5 Conclusions**

791

792 In this study, we have explored, for the first time, the possibility to infer significant trends in
793 tropospheric O₃ from the first ~10 years (January 2008 – May 2017) of IASI daily measurements
794 at a global scale. To this end, MLR analyses have been performed by applying a multivariate
795 regression model (annual and seasonal formulations), including a linear trend term in addition to
796 chemical and dynamical proxies, on gridded mean tropospheric ozone time series. This work
797 follows on the analysis of the main dynamical drivers of O₃ variations measured by IASI, which
798 was recently published in Wespes et al. (2017). We have first verified the performance of the MLR
799 models in explaining the variations in daily time series over the whole studied period. In particular,
800 we have shown that the model reproduces a large part of the O₃ variations (>70%) with small
801 residuals errors (*RMSE* of ~10%) at northern latitudes in summer. We have then performed O₃
802 trend sensitivity tests to verify the possibility to capture trend characteristics independently from
803 natural variations. Despite the weak contribution of trends to the total variation in the MLT O₃
804 columns at a global scale, the results demonstrate the possibility to discriminate significant trends
805 from the explanatory variables, especially in summer at mid-high latitudes of the N.H. (~45°N-
806 70°N) where the contribution and the sensitivity of trends are the largest (contribution of ~30-50%
807 and a ~10% increase in the *RMSE* excluding the LT in the model). We then focused on the
808 interpretation of the global trend estimates. We have found an interesting significant positive
809 trends in the S.H. tropical region extending from the Amazon to the tropical eastern Indian Ocean
810 and over South-East Asia in spring-summer which should however be carefully considered given
811 the high *RMSE* of the regression residuals in these regions. The MLR analysis reveals a band-like
812 pattern of high significant negative trends in the N.H. mid-high latitudes in summer (-0.47 ± 0.16
813 DU/yr on average in the 45°N-70°N band). The statistical significance of such trend estimates is
814 further verified by estimating, based on the autocorrelation and on the variance of the noise
815 residuals, the minimum number of years of IASI measurements that are required to detect a trend
816 of a $|5|$ DU/dec magnitude. The results clearly demonstrate the possibility to determine such a trend
817 amplitude from the available IASI dataset and the used MLR model at northern mid-high latitudes
818 in summer, while much larger measurement periods are necessary elsewhere. In particular, the
819 regions with the longest required period, in the tropics, highlight a series of known processes that
820 are closely related to the El-Niño dynamic, which underlies the lack of associated
821 parameterizations in the MLR model. The importance of using reliable MLR models in
822 understanding large-scale O₃ variations and in determining trends is further explored by comparing
823 the trends inferred from MLR and from SLR, the latter being still commonly used by the
824 international community. The comparison has clearly highlighted the gain of MLR in attributing
825 the trend-like segments in natural variations, such as ENSO, to the right processes and, hence, in
826 avoiding misinterpretation of “apparent” trends in the measurement datasets. Nevertheless, it is

827 worth noting that there could be a possible impact of the sampling (because of the cloud and quality
828 filters applied) and of the jump in September 2010 that has been identified in the IASI dataset (see
829 Section 2), in both MLR and SLR trends. Finally, by exploiting the simultaneous and vertically-
830 resolved O₃ and CO measurements from IASI, we have provided and used the O₃-CO correlations
831 in the troposphere to help determining the origins/characteristics of patterns of negative or positive
832 trends. The distributions have allowed us to identify, in particular, strong positive O₃-CO
833 correlations, regression slopes and covariance in the N.H. mid-latitudes and northward during
834 summer, which suggests a continental pollution influence in the N.H. band-like pattern of high
835 significant negative trends recorded by IASI and, hence, a direct effect of the policy measures
836 taken to reduce emissions of O₃ precursor species.

837
838 This study supports overall the importance of using (1) high density and long term homogenized
839 satellite records, such as those provided by IASI, and (2) complex models with predictor functions
840 that describe the O₃-regressors dependencies for a more accurate determination of trends in
841 tropospheric O₃ - as required by the scientific community, e.g. in the Intergovernmental Panel on
842 Climate Change (IPCC, 2013) - and for further resolving trend biases between independent
843 datasets (Payne et al., 2017; the TOAR-climate assessment report – Gaudel et al., in review).
844 Currently, no consensus in terms of O₃ trends in the troposphere is reached from the available
845 measurements (UV or IR satellites, O₃ sondes, aircrafts, ground-based measurements,...) for
846 several reasons (time-varying instrumental biases, differences in the methodology used for
847 calculating trends, in the measurement period, in the upper boundary of the O₃ columns, in the
848 retrieval algorithm, in the spatio-temporal sampling, in the vertical sensitivity of the instrument,...)
849 (Section 4.3; the TOAR-climate report – Gaudel et al., in review). However, the determination, with
850 IASI, of robust trends in tropospheric O₃ at the global scale will be achievable in the near future
851 by merging the homogeneous O₃ profiles from the three successive instruments onboard Metop-A
852 (2006); -B (2012) and -C (2018) platforms and from the IASI-Next Generation instrument onboard
853 the Metop Second Generation series of satellites (Clerbaux and Crevoisier, 2013; Crevoisier et al.,
854 2014). A long record of tropospheric O₃ measurements will be also assured by the Cross-track
855 Infrared Sounder (CrIS) onboard the Joint Polar Satellite System series of satellites.

856 857 **Acknowledgments**

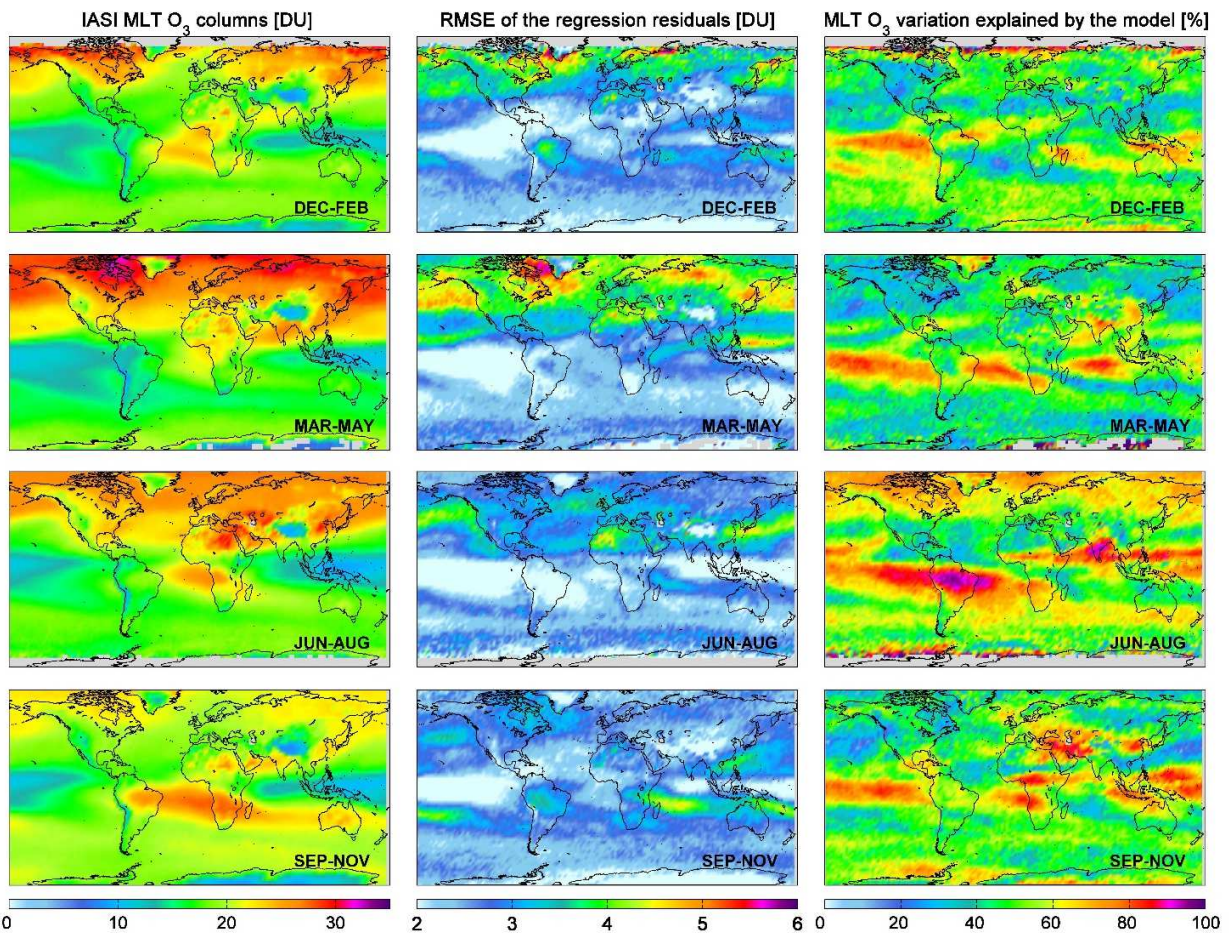
858 IASI has been developed and built under the responsibility of the Centre National d'Etudes
859 Spatiales (CNES, France). It is flown onboard the Metop satellites as part of the EUMETSAT
860 Polar System. The IASI L1 data are received through the EUMETCast near real time data
861 distribution service. We acknowledge the financial support from the ESA O₃-CCI, Copernicus O₃-
862 C3S and Eumetsat AC SAF projects. The research in Belgium is also funded by the Belgian State
863 Federal Office for Scientific, Technical and Cultural Affairs and the European Space Agency (ESA
864 Prodex IASI Flow and AC SAF).

865

866

867 **Figure captions**

868



869

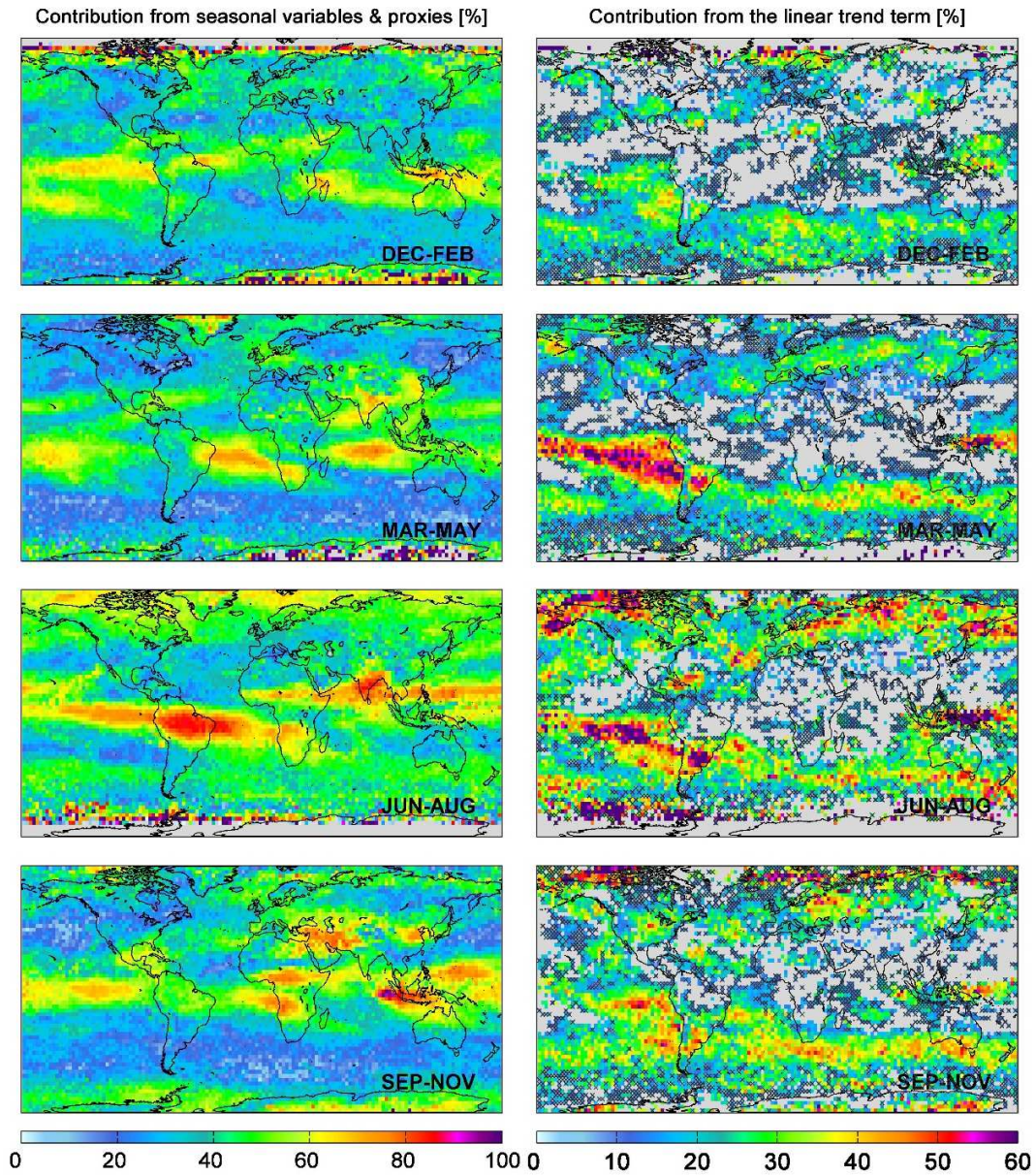
870 **Fig.1.** Seasonal distribution of O₃ tropospheric columns (in DU, integrated from ground to 300hPa)
 871 measured by IASI and averaged over January 2008 – May 2017 (left panel), of the RMSE of the
 872 regression fits (in DU, middle panel) and of the fraction of the variation in IASI data explained by
 873 the regression model, calculated as $[100 \times (\sigma(O_3^{Fitted_model}(t)) / \sigma(O_3(t)))]$ (in %, right panel). Data
 874 are averaged over a 2.5°x2.5° grid box.

875

876

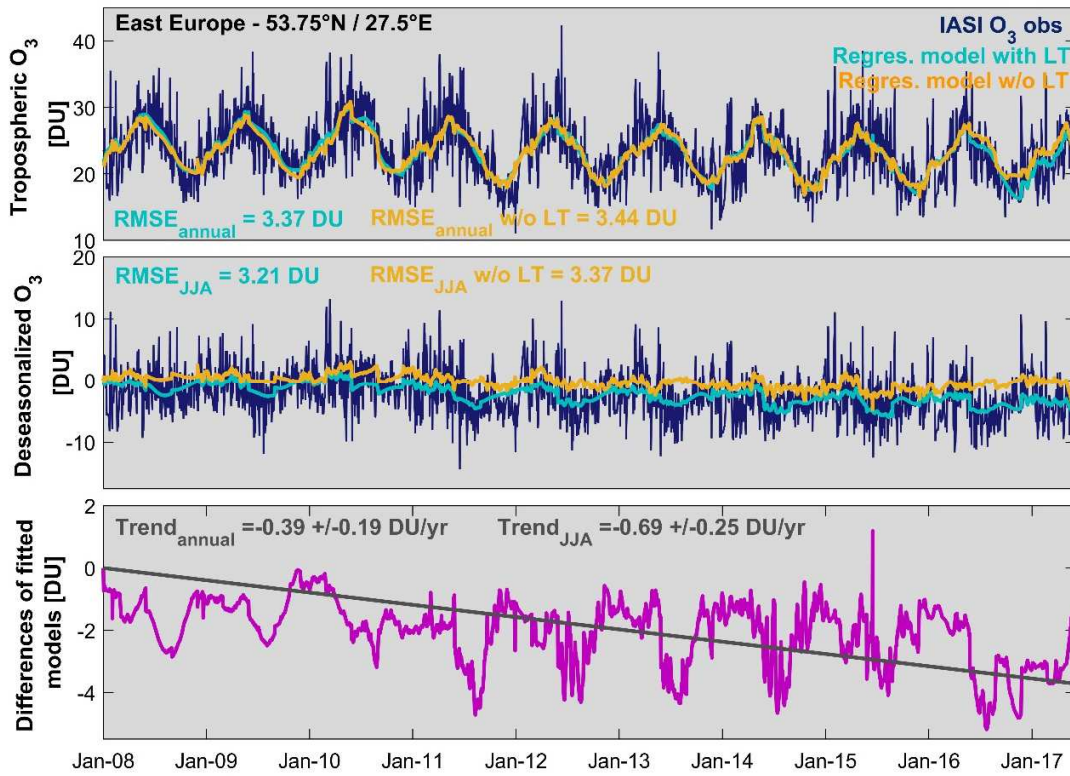
877

878

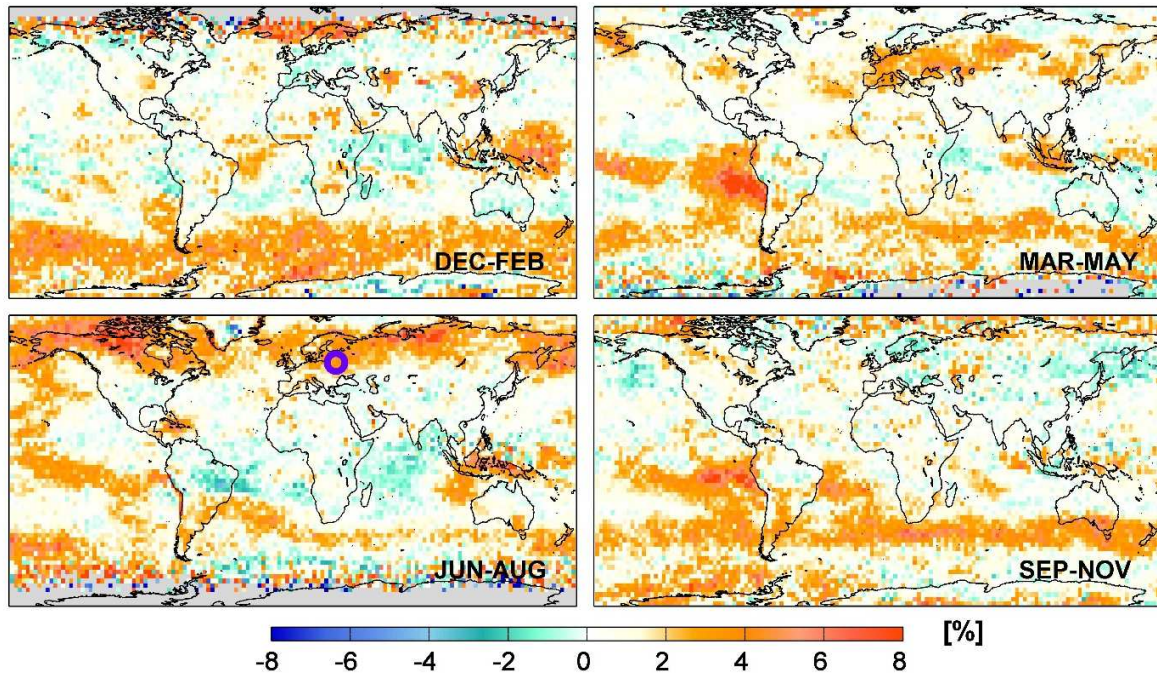


879
 880
 881
 882
 883
 884
 885
 886
 887

Fig.2. Seasonal distributions of the contribution from the seasonal and explanatory variables into the IASI O₃ variations estimated as $\left[100 \times \sigma \left(\sum_{n=1; j=2}^{4; m} [a_n; b_n; x_j] [\cos(n\omega t); \sin(n\omega t); X_{norm, j}] \right) / \sigma(O_3(t)) \right]$ (in %, left panels) and of the contribution from the linear trend calculated as $\left[100 \times \sigma(x_{j=1} \cdot trend) / \sigma(O_3(t)) \right]$ (in %, right panels). The grey areas and crosses refer to the non-significant grid cells in the 95% confidence limits (2σ level). Note that the scales are different.

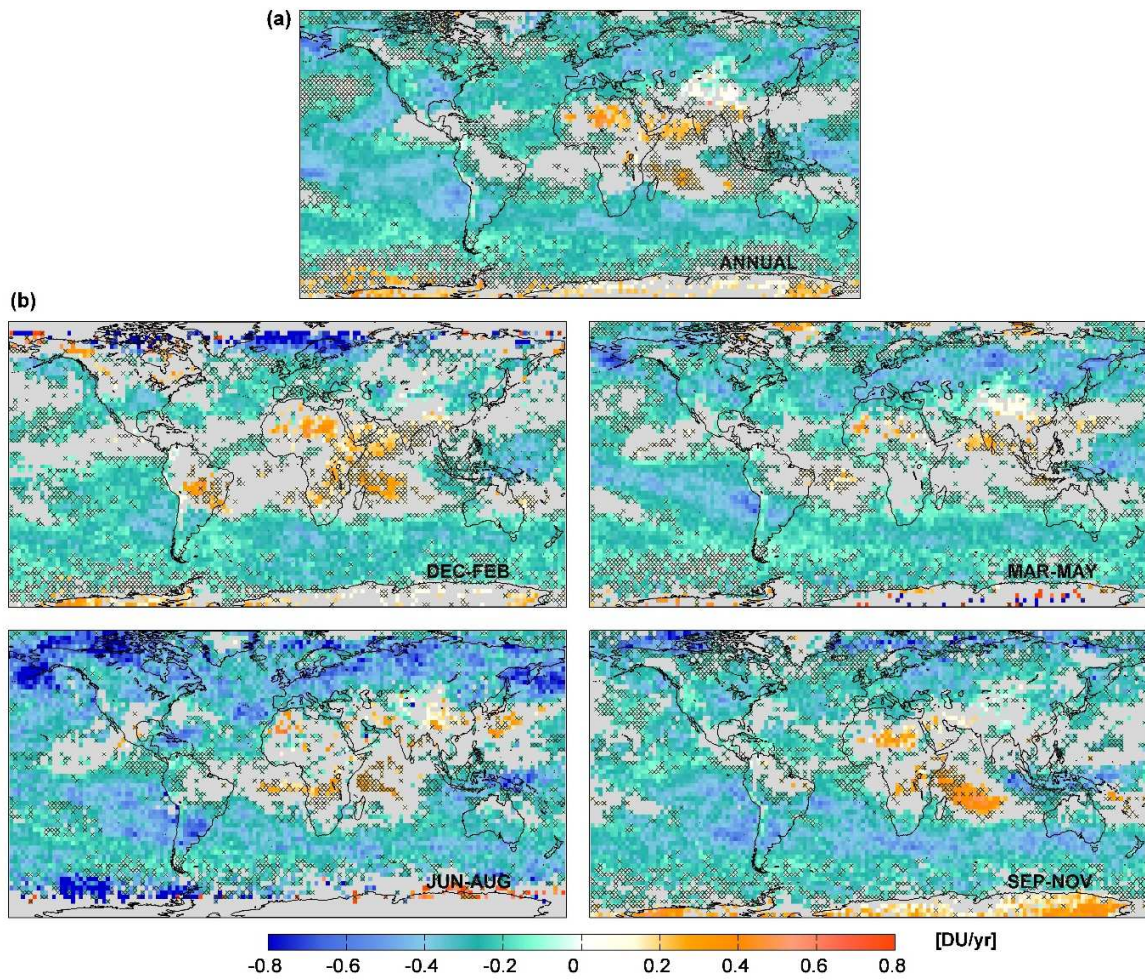


888
 889 **Fig.3.** Examples of daily time series of IASI O₃ measurements (dark blue) and of the fitted seasonal
 890 regression models with (light blue) and without (orange) the linear term in the troposphere (1st
 891 row). Daily time series of the deseasonalised O₃ (observations and regression models; 2^d row) and
 892 of the difference of the fitted models with and without the linear trend term as well as the adjusted
 893 annual trend (pink and grey lines, respectively; 3^d row) (given in DU). The *RMSE* (annual and for
 894 for the JJA period in DU) and the trend values (annual and for the JJA period in DU/yr) are also
 895 indicated.
 896
 897



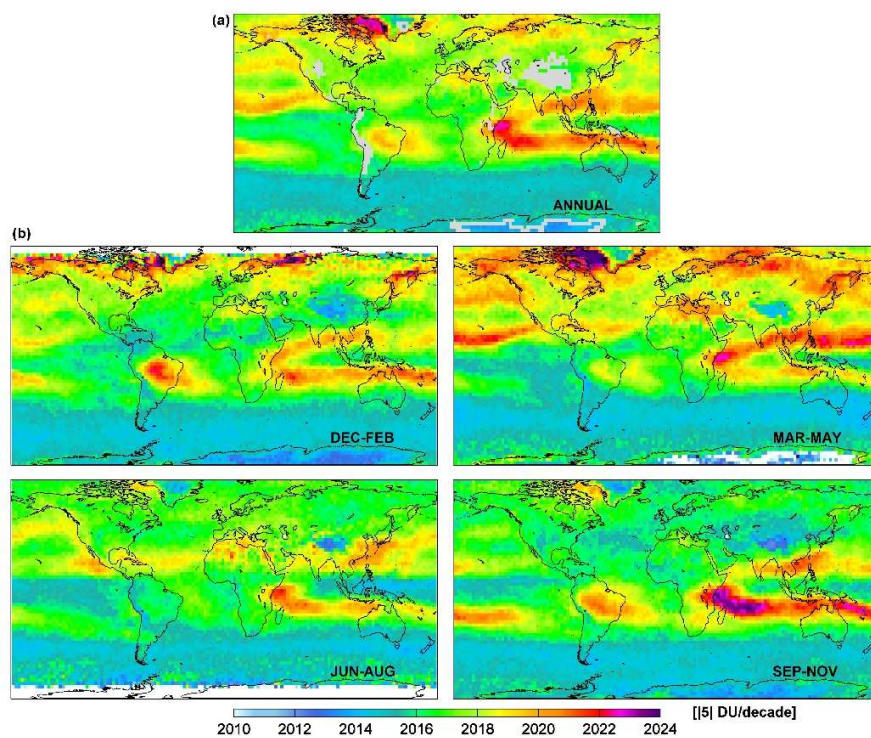
898
 899
 900
 901
 902
 903

Fig.4. Seasonal distribution of the differences between the *RMSE* of the regression fits with and without linear trend term $[(RMSE_{w/o_LT} - RMSE_{with_LT})/RMSE_{with_LT} \times 100]$ (in %). The blue circles in the JJA panel refer to the case presented in Fig.3.

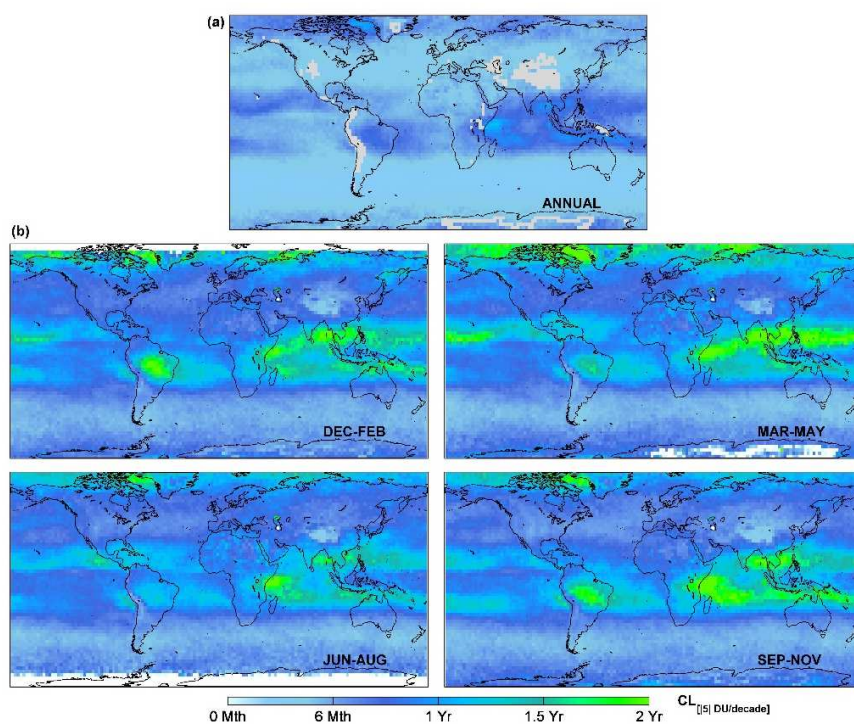


904 **Fig.5.** (a) Annual and (b) seasonal distributions of the adjusted trends in DU/yr from the multi-
 905 linear regression models. The grey areas and crosses refer to the non-significant grid cells in the
 906 95% confidence limits (2σ level).
 907

908
 909
 910

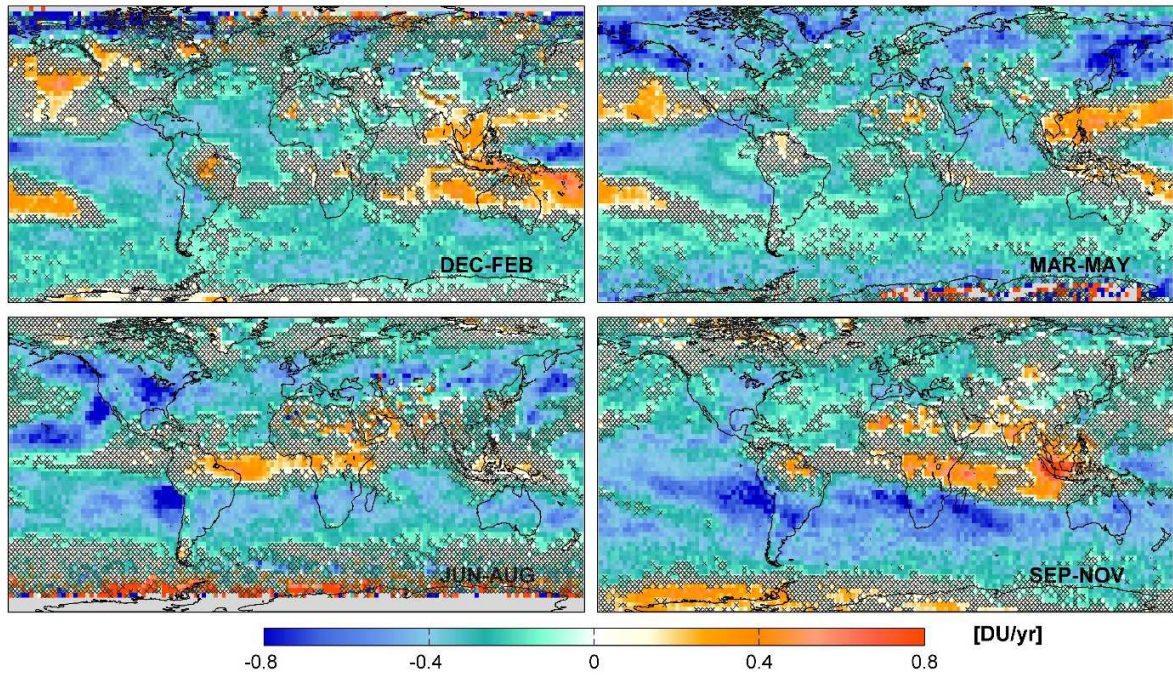


911



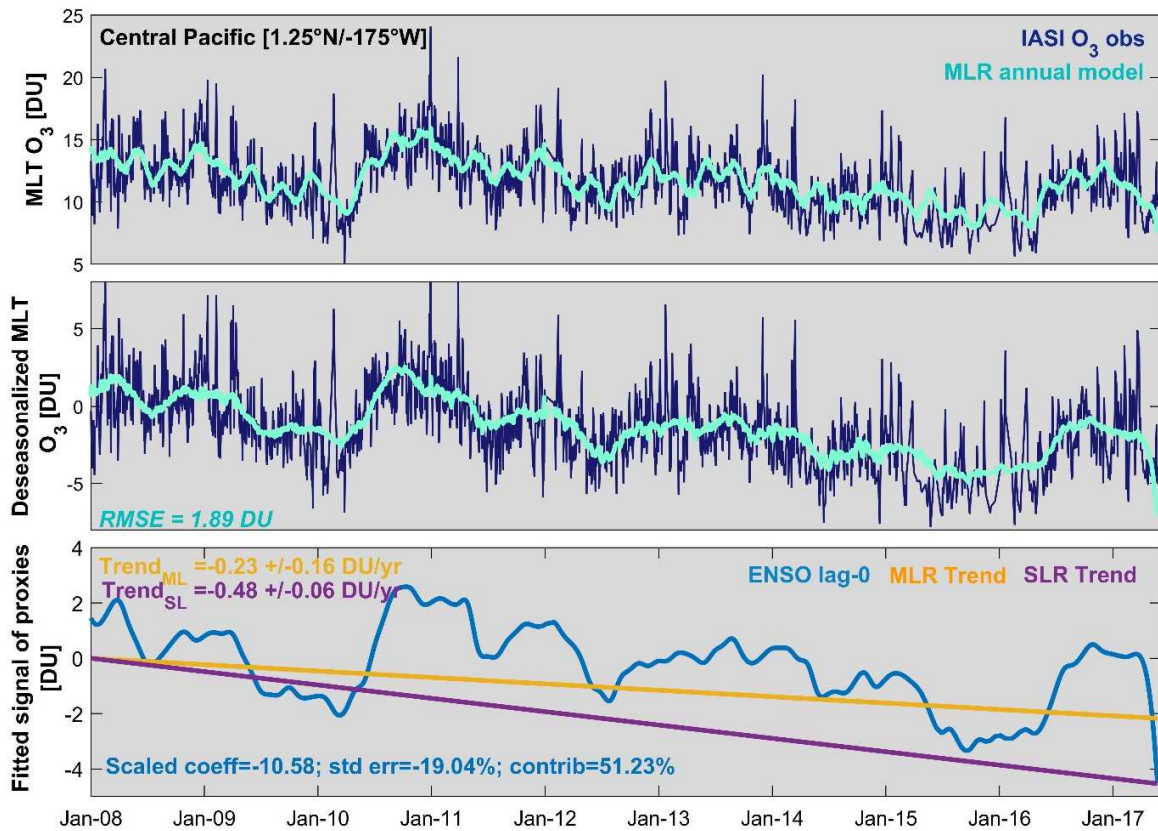
912

913 **Fig.6** (a) Estimated year of tropospheric IASI O₃ trend detection (with a probability of 90%) for a
 914 given trend of $|5|$ DU per decade starting at the beginning of the studied period (20080101) and (b)
 915 associated maximal confidence limits from the annual (top panel) and the seasonal (bottom panels)
 916 regression models.



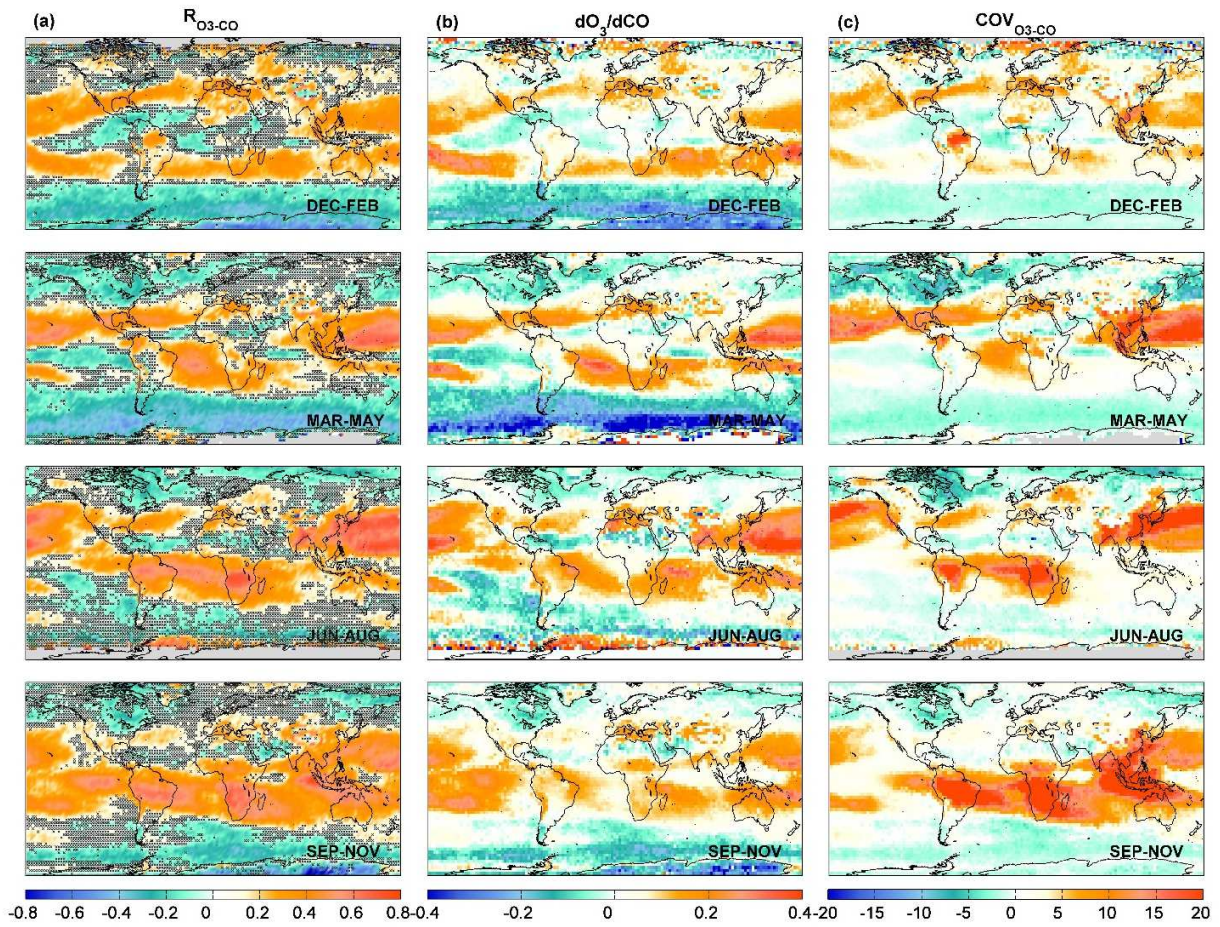
917
 918
 919
 920
 921

Fig.7. Seasonal distributions of the fitted linear term trends (given in DU/yr) derived from a single linear regression model. The crosses refer to the non-significant grid cells in the 95% confidence limits (2σ level).



922
 923 **Fig.8.** Daily time series of O₃ measured by IASI and adjusted by the multivariate annual regression
 924 model (top row and middle row for the deseasonalized O₃), along with the adjusted trends derived
 925 from the single and the multivariate linear regressions (SLR and MLR) and of the fitted signal of
 926 ENSO proxy (one of the main retained proxies in the multivariate regression model) calculated as
 927 $[x_j X_{norm,j}]$ (bottom row) over the equatorial central Pacific (negative ENSO “dynamical” effect)
 928 (given in DU). The *RMSE* of the multivariate regression fit and the fitted SLR and MLR trend
 929 values are also indicated.

930
 931
 932
 933
 934
 935



936

937 **Fig.9.** Global distributions of (a) the correlation coefficients (R_{O_3-CO}), (b) the regression slope
 938 (dO_3/dCO in $\text{mol.cm}^{-2}/\text{mol.cm}^{-2}$) and (c) the covariances (COV_{O_3-CO} in $10^{33} \text{ mol.cm}^{-2} \times \text{mol.cm}^{-2}$)
 939 of daily median IASI tropospheric O_3 and CO over January 2008 – May 2017. Data are averaged
 940 over a $2.5^\circ \times 2.5^\circ$ grid box. Crosses in R_{O_3-CO} panels (a) refer to the non-significant grid cells in the
 941 95% confidence intervals (2σ level).

942

943

944

945

946

947

948

949

950

951

952

953

954 **References**

- 955
- 956 Anton, M., D. Loyola, C. Clerbaux, M. Lopez, J. Vilaplana, M. Banon, J. Hadji-Lazaro, P. Valks,
957 N. Hao, W. Zimmer, P. Coheur, D. Hurtmans, and L. Alados-Arboledas: Validation of the Metop-
958 A total ozone data from GOME-2 and IASI using reference ground-based measurements at the
959 Iberian peninsula, *Remote Sensing of Environment*, 115, 1380-1386, 2011.
- 960
- 961 Archibald, A., Y. Elshorbany et al.: Tropospheric Ozone Assessment Report: Critical review of
962 the present-day and near future tropospheric ozone budget, *Elem. Sci. Anth.*, in-review, 2017.
- 963
- 964 Bertschi, I. T. and Jaffe, D. A.: Long-range transport of ozone, carbon monoxide, and aerosols to
965 the NE Pacific troposphere during the summer of 2003: Observations of smoke plumes from Asian
966 boreal fires, *J. Geophys. Res.*, 110(D5), D05303, doi:10.1029/2004JD005135, 2005.
- 967
- 968 Boynard, A., D. Hurtmans, M. Koukouli, et al.: Seven years of IASI ozone retrievals from FORLI:
969 validation with independent total column and vertical profile measurements, *Atmos. Meas. Tech.*,
970 9, 4327-4353, 2016.
- 971
- 972 Boynard, A., D. Hurtmans, K. Garane, F. Goutail, J. Hadji-Lazaro, M. E. Koukouli, C. Wespes,
973 A. Keppens, J.-P. Pommereau, A. Pazmino, D. Balis, D. Loyola, P. Valks, S. Hassinen, P.-F.
974 Coheur and C. Clerbaux, Validation of the IASI FORLI/Eumetsat O₃ products using satellite
975 (GOME-2), ground-based (Brewer-Dobson, SAOZ) and ozonesonde measurements, in
976 preparation for this QOS special issue.
- 977
- 978 Chen, Y., Randerson, J. T., Morton, D. C., DeFries, R. S., Collatz, G. J., Kasibhatla, P. S.,iglio,
979 L., Jin, Y., and Marlier, M. E.: Forecasting Fire Season Severity in South America Using Sea
980 Surface emperature Anomalies, *Science*, 334, 787–791, doi:10.1126/science.1209472, 2011.
- 981
- 982 Clarisse, L., Y. R'Honi ; P.-F. Coheur ; D. Hurtmans, and C. Clerbaux : Thermal infrared nadir
983 observations of 24 atmospheric gases. *Geophysical Research Letters*, 38, L10802, 2011.
- 984
- 985 Clerbaux, C., A. Boynard, L. Clarisse, M. George, J. Hadji-Lazaro, H. Herbin, D. Hurtmans, M.
986 Pommier, A. Razavi, S. Turquety, C. Wespes, and P.-F. Coheur: Monitoring of atmospheric
987 composition using the thermal infrared IASI/MetOp sounder, *Atmos. Chem. Phys.*, 9, 6041-6054,
988 2009.
- 989
- 990 Clerbaux C. and C. Crevoisier: New Directions: Infrared remote sensing of the troposphere from
991 satellite: Less, but better, *Atmospheric Environment*, 72, 24-26, 2013.
- 992
- 993 Crevoisier, C., Clerbaux, C., Guidard, V., Phulpin, T., Armante, R., Barret, B., Camy-Peyret, C.,
994 Chaboureaud, J.-P., Coheur, P.-F., Crépeau, L., Dufour, G., Labonnote, L., Lavanant, L., Hadji-
995 Lazaro, J., Herbin, H., Jacquinet-Husson, N., Payan, S., Péquignot, E., Pierangelo, C., Sellitto, P.,
996 and Stubenrauch, C. : Towards IASI-New Generation (IASI-NG): impact of improved spectral
997 resolution and radiometric noise on the retrieval of thermodynamic, chemistry and climate
998 variables, *Atmos. Meas. Tech.*, 7, 4367-4385, 2014.

999
1000 Cohen, Y., et al.: Climatology and long-term evolution of ozone and carbon monoxide in the UTLS
1001 at northern mid-latitudes, as seen by IAGOS from 1995-2013, ACPD, in-review, 2017.
1002
1003 Cooper, O., D. Parrish, A. Stohl, M. Trainer, P. Nédélec, V. Thouret, J.-P. Cammas, S. Oltmans,
1004 B. Johnson and D. Tarasick: Increasing springtime ozone mixing ratios in the free troposphere
1005 over western North America, *Nature*, 463, 344–348, doi:10.1038/nature08708, 2010.
1006
1007 Cooper, O. R., R.-S. Gao, D. Tarasick, T. Leblanc, and C. Sweeney: Long-term ozone trends at
1008 rural ozone monitoring sites across the United States, 1990–2010, *J. Geophys. Res.*, 117, D22307,
1009 doi:10.1029/2012JD018261, 2012.
1010
1011 Cooper, O. R., D. D. Parrish, J. Ziemke, N. V. Balashov, M. Cupeiro, I. E. Galbally, S. Gilge, L.
1012 Horowitz, N. R. Jensen, J.-F. Lamarque, V. Naik, S. J. Oltmans, J. Schwab, D. T. Shindell, A. M.
1013 Thompson, V. Thouret, Y. Wang, R. M. Zbinden: Global distribution and trends of tropospheric
1014 ozone: An observation-based review, *Elementa: Science of the Anthropocene*, 2, 000029,
1015 doi:10.12952/journal.elementa.000029, 2014.
1016
1017 Doughty, D. C., Thompson, A. M., Schoeberl, M. R., Stajner, I., Wargan, K., and Hui, W. C. J.:
1018 An intercomparison of tropospheric ozone retrievals derived from two Aura instruments and
1019 measurements in western North America in 2006, *J. Geophys. Res.*, 116,
1020 D06303, doi:10.1029/2010JD014703, 2011.
1021
1022 Dufour, G., M. Eremenko, A. Griesfeller, B. Barret, E. LeFlochmoen, C. Clerbaux, J. Hadji-
1023 Lazaro, P.-F. Coheur, and D. Hurtmans: Validation of three different scientific ozone products
1024 retrieved from IASI spectra using ozonesondes, *Atmos. Meas. Tech.*, 5, 611-630, 2012.
1025
1026 Duncan, B. N., Lamsal, L. N., Thompson, A. M., Yoshida, Y., Lu, Z., Streets, D. G., Hurwitz, M.
1027 M., and Pickering, K. E.: A space-based, high-resolution view of notable changes in urban
1028 NO_x pollution around the world (2004-2005), *J. Geophys. Res.* 121, 976–96, 2016.
1029
1030 [Ebojje, F., Burrows, J. P., Gebhardt, C., Ladstätter-Weissenmayer, A., von Savigny, C., Rozanov,](#)
1031 [A., Weber, M., and Bovensmann, H.: Global tropospheric ozone variations from 2003 to 2011 as](#)
1032 [seen by SCIAMACHY, *Atmos. Chem. Phys.*, 16, 417-436, doi:10.5194/acp-16-417-2016, 2016.](#)
1033
1034 Fishman, J., K. Fakhruzzaman, B. Cros and D. Nganda: Identification of widespread pollution in
1035 the southern-hemisphere deduced from satellite analyses, *Science*, 252, 1693-1696, 1991.
1036
1037 Fishman, J., Creilson, J. K., Wozniak, A. E., and Crutzen, P. J.: Interannual variability of
1038 stratospheric and tropospheric ozone determined from satellite measurements, *J. Geophys. Res.*,
1039 110, D20306, doi:10.1029/2005JD005868, 2005.
1040
1041 Frossard, L., H.E. Rieder, M. Ribatet, J. Staehelin, J. A. Maeder, S. Di Rocco, A. C. Davison, T.
1042 Pete.: On the relationship between total ozone and atmospheric dynamics and chemistry at mid-

1043 latitudes – Part 1: Statistical models and spatial fingerprints of atmospheric dynamics and
1044 chemistry, *Atmos. Chem. Phys.*, 13, 147–164, doi:10.5194/acp-13-147-2013, 2013.
1045
1046 Fusco, A. C., and J. A. Logan: Analysis of 1970–1995 trends in tropospheric ozone at northern
1047 hemisphere midlatitudes with the GEOSCHEM model, *J. Geophys. Res.*, 108(D15), 4449,
1048 doi:10.1029/2002JD002742, 2003.
1049
1050 Gaudel, A., O. R. Cooper, G. Ancellet, B. Barret, A. Boynard, J. P. Burrows, C. Clerbaux, P.-F.
1051 Coheur, J. Cuesta, E. Cuevas, S. Doniki, G. Dufour, F. Ebojie, G. Foret, O. Garcia, M. J. Granados-
1052 Muñoz, J. Hannigan, F. Hase, B. Hassler, G. Huang, D. Hurtmans, D. Jaffe, N. Jones, P.
1053 Kalabokas, B. Kerridge, S. Kulawik, B. Latter, T. Leblanc, E. Le Flochmoën, W. Lin, J. Liu, X.
1054 Liu, E. Mahieu, A. McClure-Begley, J. Neu, M. Osman, M. Palm, H. Petetin, I. Petropavlovskikh,
1055 R. Querel, N. Rahpoe, A. Rozanov, M. G. Schultz, J. Schwab, R. Siddans, D. Smale, M.
1056 Steinbacher, H. Tanimoto, D. Tarasick, V. Thouret, A. M. Thompson, T. Trickl, E. Weatherhead,
1057 C. Wespes, H. Worden, C. Vigouroux, X. Xu, G. Zeng, J. Ziemke: Tropospheric Ozone
1058 Assessment Report: Present-day distribution and trends of tropospheric ozone relevant to climate
1059 and global atmospheric chemistry model evaluation, submitted to Elementa.
1060
1061 Gazeaux, J., C. Clerbaux, M. George, J. Hadji-Lazaro, J. Kuttippurath, P.-F. Coheur, D. Hurtmans,
1062 T. Deshler, M. Kovilakam, P. Campbell, V. Guidard, F. Rabier, and J.-N. Thepaut:
1063 Intercomparison of polar ozone profiles by IASI/Metop sounder with 2010 concordiasi
1064 ozonesonde observations, *Atmos. Meas. Tech.*, 5, 7923-7944, 2012.
1065
1066 Hess, P.G. and R. Zbinden: Stratospheric impact on tropospheric ozone variability and trends:
1067 1990–200, *Atmos. Chem. Phys.*, 13, 649–674, 2013.
1068
1069 [Heue, K.-P., Coldewey-Egbers, M., Delcloo, A., Lerot, C., Loyola, D., Valks, P., and van](#)
1070 [Roozendael, M.: Trends of tropical tropospheric ozone from 20 years of European satellite](#)
1071 [measurements and perspectives for the Sentinel-5 Precursor, *Atmos. Meas. Tech.*, 9, 5037-5051,](#)
1072 [doi:10.5194/amt-9-5037-2016, 2016.](#)
1073
1074 Hilton, F., R. Armante, T. August, et al. : Hyperspectral Earth Observation from IASI: Five Years
1075 of Accomplishments, *Bulletin of the American Meteorological Society*, vol. 93, issue 3, pp. 347-
1076 370, 2012.
1077
1078 Hurtmans, D., P. Coheur, C. Wespes, L. Clarisse, O. Scharf, C. Clerbaux, J. Hadji-Lazaro, M.
1079 George, and S. Turquety: FORLI radiative transfer and retrieval code for IASI, *Journal of*
1080 *Quantitative Spectroscopy and Radiative Transfer*, 113, 1391-1408, 2012.
1081
1082 Intergovernmental Panel on Climate Change, *Climate Change 2013: The Physical Science Basis.*
1083 *Contribution of Working Group I to the Fifth Assessment Report of the Intergovernmental Panel*
1084 *on Climate Change*, edited by T. F. Stocker et al., pp. 164–270, Cambridge Univ. Press,
1085 Cambridge, U. K., and New York, 2013.
1086

1087 Jonson, J. E., Simpson, D., Fagerli, H., and Solberg, S.: Can we explain the trends in European
1088 ozone levels?, *Atmos. Chem. Phys.*, 6, 51–66, doi:10.5194/acp-6-51-2006, 2006.
1089

1090 Keppens, A., J.-C. Lambert, J. Granville, D. Hubert, T. Verhoelst, S. Compernelle, B. Latter, B.
1091 Kerridge, R. Siddans, A. Boynard, J. Hadji-Lazaro, C. Clerbaux, C. Wespes, D. R. Hurtmans, P.-
1092 F. Coheur, J. van Peet, R. van der A, K. Garane, M. E. Koukouli, D. S. Balis, A. Delcloo, R. Kivi,
1093 R. Stübi, S. Godin-Beekmann, M. Van Roozendael, C. Zehner: Quality assessment of the
1094 Ozone_cci Climate Research Data Package (release 2017): 2. Ground-based validation of nadir
1095 ozone profile data products, in preparation for this QOS special issue.
1096

1097 Kim, P. S., D. J. Jacob, X. Liu, J. X. Warner, K. Yang, K. Chance, V. Thouret, and P. Nedelec:
1098 Global ozone–CO correlations from OMI and AIRS: constraints on tropospheric ozone sources,
1099 *Atmos. Chem. Phys.*, 13, 9321–9335, 2013.
1100

1101 Knibbe J. S., R. J. van der A, and A. T. J. de Laat: Spatial regression analysis on 32 years of total
1102 column ozone data, *Atmos. Chem. Phys.*, 14, 8461–8482, 2014.
1103

1104 Krotkov, N. A., McLinden, C. A., Li, C., Lamsal, L. N., Celarier, E. A., Marchenko, S. V., Swartz,
1105 W. H., Bucsela, E. J., Joiner, J., Duncan, B. N., Boersma, K. F., Veeffkind, J. P., Levelt, P. F.,
1106 Fioletov, V. E., Dickerson, R. R., He, H., Lu, Z., and Streets, D. G.: Aura OMI observations of
1107 regional SO₂ and NO₂ pollution changes from 2005 to 2015, *Atmos. Chem. Phys.*, 16, 4605–4629,
1108 doi:10.5194/acp-16-4605-2016, 2016.
1109

1110 Labrador, L. J., von Kuhlmann, R., and Lawrence, M. G.: Strong sensitivity of the global mean
1111 OH concentration and the tropospheric oxidizing efficiency to the source of NO_x from lightning,
1112 *Geophys. Res. Lett.*, 31, L06102, doi:10.1029/2003GL019229, 2004.
1113

1114 Leventidou, E., Weber, M., Eichmann, K.-U., and Burrows, J. P.: Harmonisation and trends of 20-
1115 years tropical tropospheric ozone data, *Atmos. Chem. Phys. Discuss.*, [https://doi.org/10.5194/acp-](https://doi.org/10.5194/acp-2017-815)
1116 2017-815, in review, 2017.
1117

1118 Lewis, S. L., Brando, P. M., Phillips, O. L., van der Heijden, G. M. F., and Nepstad, D.: The 2010
1119 Amazon Drought, *Science*, 331, 554–554, doi:10.1126/science.1200807, 2011.
1120

1121 Liang, Q., Jaegle, L., Hudman, R. C., Turquety, S., Jacob, D. J., Avery, M. A., Browell, E. V.,
1122 Sachse, G. W., Blake, D. R., Brune, W., Ren, X., Cohen, R. C., Dibb, J. E., Fried, A., Fuelberg,
1123 H., Porter, M., Heikes, B. G., Huey, G., Singh, H. B., and Wennberg, P. O.: Summertime influence
1124 of Asian pollution in the free troposphere over North America, *J. Geophys. Res.*, 112, D12S11,
1125 doi:10.1029/2006JD007919, 2007.
1126

1127 Lin, M., L. W. Horowitz, O. R. Cooper, D. Tarasick, S. Conley, L. T. Iraci, B. Johnson, T. Leblanc,
1128 I. Petropavlovskikh, and E. L. Yates: Revisiting the evidence of increasing springtime ozone
1129 mixing ratios in the free troposphere over western North America, *Geophys. Res. Lett.*, 42, 8719–
1130 8728, doi:10.1002/2015GL065311, 2015.
1131

1132 Liu, X., P. K. Bhartia, K. Chance, R. J. D. Spurr, and T. P. Kurosu: Ozone profile retrievals from
1133 the Ozone Monitoring Instrument, *Atmos. Chem. Phys.*, 10, 2521–2537, 2010.
1134
1135 Liu, J., Rodriguez, J. M., Thompson, A. M., Logan, J. A., Douglass, A. R., Olsen, M. A., Steenrod,
1136 S. D., and Posny, F.: Origins of tropospheric ozone interannual variation over Reunion: A model
1137 investigation, *J. Geophys. Res.-Atmos.*, 121, 521–537, doi:10.1002/2015jd023981, 2016.
1138
1139 Liu, J., et al.: Causes of interannual variability over the southern hemispheric tropospheric ozone
1140 maximum, *Atmos. Chem. Phys.*, 17, 3279–3299, 2017.
1141
1142 Logan, J. A., M. J. Prather, S. C. Wofsy, and M. B. McElroy: Tropospheric chemistry: A global
1143 perspective, *J. Geophys. Res.*, 86 (NC8), 7210–7254, doi:10.1029/JC086iC08p07210, 1981.
1144
1145 Logan, J. A.: Tropospheric Ozone: Seasonal behaviour, Trends, and Anthropogenic Influence, *J.*
1146 *Geophys. Res.*, 90(D6), 10 463–10 482, 1985.
1147
1148 Logan, J. A., and V. W. J. H. Kirchhoff: Seasonal variations of tropospheric ozone at Natal, Brazil,
1149 *J. Geophys. Res.*, 91(D7), 7875–7881, doi:10.1029/JD091iD07p07875, 1986.
1150
1151 Logan, J. A., Staehelin, J., Megretskaia, I. A., Cammas, J.-P., Thouret, V., Claude, H., De Backer,
1152 H., Steinbacher, M., Scheel, H.-E., Stübi, R., Fröhlich, M., and Derwent, R.: Changes in ozone
1153 over Europe: Analysis of ozone measurements from sondes, regular aircraft (MOZAIC) and alpine
1154 surface sites, *J. Geophys. Res.*, doi:10.1029/2011JD016952, 2012.
1155
1156 Mäder, J. A., J. Staehelin, D. Brunner, W.A. Stahel, I. Wohltmann, and T. Peter: Statistical
1157 modelling of total ozone: Selection of appropriate explanatory variables, *J. Geophys. Res.*, 112,
1158 D11108, doi:10.1029/2006JD007694, 2007.
1159
1160 Miyazaki et al.: Decadal changes in global surface NO_x emission from multi-constituent satellite
1161 data assimilation, *Atmos. Chem. Phys.*, 17, 807–837, 2017.
1162
1163 Moxim, W. J., and H. Levy II: A model analysis of the tropical South Atlantic Ocean tropospheric
1164 ozone maximum: The interaction of transport and chemistry, *J. Geophys. Res.*, 105(D13), 17393–
1165 17415, doi:10.1029/2000JD900175, 2000.
1166
1167 Neu, J.L., T. Flury, G. L. Manney, M. L. Santee, N. J. Livesey and J. Worden, Tropospheric ozone
1168 variations governed by changes in stratospheric circulation, *Nat. Geosc.*, 7, 340–344,
1169 doi:10.1038/ngeo2138, 2014.
1170
1171 Oetjen, H., Payne, V.H., Kulawik, S.S., Eldering, A., Worden, J., Edwards, D.P., Francis, G.L.,
1172 Worden, H.M., Clerbaux, C., Hadji-Lazaro, J., Hurtmans, D. : Extending the satellite data record
1173 of tropospheric ozone profiles from Aura-TES to MetOp-IASI, *Atmos. Meas. Tech.*, 7, 4223–4236,
1174 doi:10.5194/amt-7-4223-2014, 2014.
1175

1176 Oltmans, S.J, A. S. Lefohn; D. Shadwick, J. M. Harris, H.-E. Scheel, I. Galbally, D. W. Tarasick,
1177 B. J. Johnson, E.G. Brunke, H. Claude, G. Zeng, S. Nichol, F.J. Schmidlin, J. Davies, E. Cuevas,
1178 A. Redondas, H. Naoe, T. Nakano, T. Kawasato: Recent Tropospheric Ozone Changes - A Pattern
1179 Dominated by Slow or No Growth, *Atmospheric Environment*, 67, p. 331-351,
1180 10.1016/j.atmosenv.2012.10.057, 2013.
1181
1182 Oman, L. D., Douglass, A. R., Ziemke, J. R., Rodriguez, J. M., Waugh, D. W., and Nielsen, J. E.:
1183 The ozone response to ENSO in Aura satellite measurements and a chemistry–climate simulation,
1184 *J. Geophys. Res.-Atmos.*, 118, 965–976, 2013.
1185
1186 Parrington, M., P. I. Palmer, D. K. Henze, D. W. Tarasick, E. J. Hyer, R. C. Owen, D. Helmig, C.
1187 Clerbaux, K. W. Bowman, M. N. Deeter, E. M. Barratt, P.-F. Coheur, D. Hurtmans, Z. Jiang, M.
1188 George, and J. R. Worden: The influence of boreal biomass burning emissions on the distribution
1189 of tropospheric ozone over north America and the north Atlantic during 2010, *Atmos. Chem.*
1190 *Phys.*, 12, 2077-2098, doi: 10.5194/acp-12-2077-2012, 2012.
1191
1192 Parrish, D.D., Holloway, J.S., Trainer, M., Murphy, P.C., Forbes, G.L., and Fehsenfeld, F.C.:
1193 Export of North American Ozone Pollution to the North Atlantic Ocean, *Science*, 259, 1436–1439,
1194 1993.
1195
1196 Parrish, D.D., K.S. Law, J. Staehelin, R. Derwent, O.R. Cooper, et al.: Long-term changes in lower
1197 tropospheric baseline ozone concentrations at northern mid-latitudes. *Atmos. Chem. Phys* 12:
1198 11485–11504. doi:10.5194/acp-12-11485-2012, 2012.
1199
1200 Payne, V. H., J. L. Neu and H. M. Worden: Satellite observations for understanding the drivers of
1201 variability and trends in tropospheric ozone, *J. Geophys. Res.*, in-press, 2017.
1202
1203 Pommier, M., C. Clerbaux, K. S. Law, G. Ancellet, P. Bernath, P.-F. Coheur, J. Hadji- Lazaro, D.
1204 Hurtmans, P. Nedelec, J.-D. Paris, F. Ravetta, T. B. Ryerson, H. Schlager, and A. J. Weinheimer:
1205 Analysis of IASI tropospheric O₃ data over the arctic during POLARCAT campaigns in 2008,
1206 *Atmos. Chem. Phys.*, 12, 7371-7389, doi:doi:10.5194/acp-12-7371-2012, 2012.
1207
1208 Rieder, H. E., Frossard, L., Ribatet, M., Staehelin, J., Maeder, J. A., Di Rocco, S., Davison, A. C.,
1209 Peter, T., Weihs, P., and Holawe, F.: On the relationship between total ozone and atmospheric
1210 dynamics and chemistry at mid-latitudes – Part 2: The effects of the El Nino/Southern Oscillation,
1211 volcanic eruptions and contributions of atmospheric dynamics and chemistry to long-term total
1212 ozone changes, *Atmos. Chem. Phys.*, 13, 165–179, 2013.
1213
1214 Rodgers, C. D.: *Inverse Methods for Atmospheric Sounding: Theory and Practice*, World
1215 Scientific, Series on Atmospheric, Oceanic and Planetary Physics, 2, Hackensack, N. J., 2000.
1216
1217 Safieddine, S., Boynard, A., Coheur, P.-F., Hurtmans, D., Pfister, G., Quennehen, B., Thomas, J.
1218 L., Raut, J.-C., Law, K. S., Klimont, Z., Hadji-Lazaro, J., George, M., and Clerbaux, C.:
1219 Summertime tropospheric ozone assessment over the Mediterranean region using the thermal

1220 infrared IASI/MetOp sounder and the WRF-Chem model, *Atmos. Chem. Phys.*, 14, 10119–10131,
1221 doi:10.5194/acp-14-10119-2014, 2014.
1222
1223 Saunio, M., Emmons, L., Lamarque, J.-F., Tilmes, S., Wespes, C., Thouret, V., and Schultz, M.:
1224 Impact of sampling frequency in the analysis of tropospheric ozone observations, *Atmos. Chem.*
1225 *Phys.*, 12, 6757–6773, doi:10.5194/acp-12-6757-2012, 2012.
1226
1227 Sauvage, B., Thouret, V., Thompson, A. M., Witte, J. C., Cammas, J. P., Nedelec, P., and Athier,
1228 G.: Enhanced view of the “tropical Atlantic ozone paradox” and “zonal wave one” from the in situ
1229 MOZAIC and SHADOZ data, *J. Geophys. Res.-Atmos.*, 111, D01301,
1230 doi:10.1029/2005jd006241, 2006.
1231
1232 Sauvage, B., Martin, R. V., van Donkelaar, A., and Ziemke, J. R.: Quantification of the factors
1233 controlling tropical tropospheric ozone and the South Atlantic maximum, *J. Geophys. Res.-*
1234 *Atmos.*, 112, D11309, doi:10.1029/2006jd008008, 2007.
1235
1236 Scannell, C., D. Hurtmans, A. Boynard, J. Hadji-Lazaro, M. George, A. Delcloo, A. Tuinder, P.F.
1237 Coheur, and C. Clerbaux: Antarctic ozone hole as observed by IASI/MetOp for 2008–2010, *Atmos.*
1238 *Meas. Tech.*, 5, 123–139, 2012.
1239
1240 Simon, H., A. Reff, B. Wells, J. Xing, and N. Frank: Ozone Trends Across the United States over
1241 a Period of Decreasing NO_x and VOC Emissions, *Environ. Sci. Technol.*, 49, 186–195,
1242 dx.doi.org/10.1021/es504514z, 2015.
1243
1244 Stohl, A., S. Eckhardt, C. Forster, P. James, and N. Spichtinger: On the pathways and timescales
1245 of intercontinental air pollution transport. *J. Geophys. Res.* 107 (D23), 4684,
1246 doi:10.1029/2001JD001396, 2002.
1247
1248 Thompson, D. W. J. and J.M. Wallace: Annular modes in the extratropical circulation. Part I:
1249 month-to-month variability, *J. Climate*, 13, 1000–1016, 2000.
1250
1251 Thompson, A.M., J.C. Witte, H.G.J. Smit, S.J. Oltmans, B.J. Johnson, V.W.J H. Kirchhoff, and
1252 F.J. Schmidlin: Southern Hemisphere Additional Ozonesondes (SHADOZ) 1998–2004 tropical
1253 ozone climatology: 3. Instrumentation, station-to-station variability, and evaluation with simulated
1254 flight profiles, *J. Geophys. Res.*, 112, D03304, doi:10.1029/2005JD007042, 2007.
1255
1256 Tarasick et al.: Tropospheric Ozone Assessment Report: Tropospheric ozone observations, *Elem.*
1257 *Sci. Anth.*, in-review, 2017.
1258
1259 Thouret, V., J.-P. Cammas, B. Sauvage, G. Athier, R. Zbinden, R., P. Nédélec, P. Simon, and F.
1260 Karcher: Tropopause referenced ozone climatology and inter-annual variability (1994–2003) from
1261 the MOZAIC programme, *Atmos. Chem. Phys.*, 6, 1033–1051, doi:10.5194/acp-6-1033-2006,
1262 2006.
1263

1264 Tiao, G. C., G. C. Reinsel, D. Xu, J. H. Pedrick, X. Zhu, A. J. Miller, J. J. DeLuisi, C. L. Mateer,
1265 and D. J. Wuebbles, Effects of autocorrelation and temporal sampling schemes on estimates of
1266 trend and spatial correlation, *J. Geophys. Res.*, 95, 20,507–20,517, 1990.

1267

1268 Tocquer, F., Barret, B., Mari, C., Le Flochmoen, E., Cammas, J. P., and Sauvage, B.: An upper
1269 tropospheric 'ozone river' from Africa to India during the 2008 Asian post-monsoon season, *Tellus*
1270 *B*, 67, 25350, doi:10.3402/tellusb.v67.25350, 2015.

1271

1272 Valks, P., N. Hao, S. Gimeno Garcia, D. Loyola, M. Dameris, P. Jöckel, and A. Delcloo: Tropical
1273 tropospheric ozone column retrieval for GOME-2, *Atmos. Meas. Tech.*, 7, 2513–2530,
1274 doi:10.5194/amt-7-2513-2014, 2014.

1275

1276 Van der A, R. J., et al.: Cleaning up the air: effectiveness of air quality policy for SO₂ and NO_x
1277 emissions in China, *Atmos. Chem. Phys.*, 17, 1775–1789, 2017.

1278

1279 Verstraeten, W.W., J.L. Neu, J.E. Williams, K.W. Bowman, J.R. Worden and K.F. Boersma:
1280 Rapid increases in tropospheric ozone production and export from China, *Nature Geosciences*,
1281 doi: 10.1038/NGEO2493, 2015.

1282

1283 Voulgarakis, A., Telford, P. J., Aghedo, A. M., Braesicke, P., Faluvegi, G., Abraham, N. L.,
1284 Bowman, K. W., Pyle, J. A., and Shindell, D. T.: Global multi-year O₃-CO correlation patterns
1285 from models and TES satellite observations, *Atmos. Chem. Phys.*, 11, 5819–5838,
1286 doi:10.5194/acp-10-2491-2010, 2010.

1287

1288 Voulgarakis, A., P. Hadjinicolaou, J. A. Pyle: Increases in global tropospheric ozone following an
1289 El Nino event: examining stratospheric ozone variability as a potential driver, *Atmos. Sci. Lett.* 12:
1290 228–232, doi: 10.1002/asl.318, 2011.

1291

1292 Weatherhead, E.C., G. C. Reinsel, G. C. Tiao, X.-L. Meng, D. Choi, W.-K. Cheang, T. Keller, J.
1293 DeLuisi, D. J. Wuebbles, J. B. Kerr, A. J. Miller, S. J. Oltmans and J. E. Frederick: Factors
1294 affecting the detection of trends: Statistical considerations and applications to environmental data,
1295 *J. Geophys. Res. Atmos.*, 103, 17149–17161, 1998.

1296

1297 Wespes, C., D. Hurtmans, L.K. Emmons, S. Safieddine, C. Clerbaux, D.P. Edwards, and P.-F.
1298 Coheur: Ozone variability in the troposphere and the stratosphere from the first six years of IASI
1299 observations (2008–2013), *Atmos. Chem. Phys.*, 16, 5721–5743, 2016.

1300

1301 Wespes, C., D. Hurtmans, C. Clerbaux, and P.-F. Coheur: O₃ variability in the troposphere as
1302 observed by IASI over 2008–2016 — Contribution of atmospheric chemistry and dynamics, *J.*
1303 *Geophys. Res. Atmos.*, 122, 2429–2451, doi:10.1002/2016JD025875, 2017.

1304

1305 Wilson, R. C., Z.L. Fleming, P.S. Monks, G. Clain, S.Henne, I.B. Konovalov, S. Szopa, and L.
1306 Menut: Have primary emission reduction measures reduced ozone across Europe? An analysis of
1307 European rural background ozone trends 1996–2005, *Atmos. Chem. Phys.*, 12, 437–454,
1308 doi:10.5194/acp-12-437-2012, 2012.

1309
1310 Worden, J., Jiang, Z., Jones, D.B.A., Alvarado, M., Bowman, K., Frankenberg, C., Kort, E.A.,
1311 Kulawik, S., S., Lee, M., Liu, J., Payne, V., Wecht, K., Worden, H.: El Niño, the 2006 Indonesian
1312 peat fires, and the distribution of atmospheric methane, *Geophys. Res. Lett.*, V40, 1–6,
1313 doi:10.1002/grl.50937, 2013.
1314
1315 Zbinden, R. M., J.-P. Cammas, V. Thouret, P. Nédélec, F. Karcher, and P. Simon: Mid-latitude
1316 tropospheric ozone columns from the MOZAIC program: climatology and interannual variability,
1317 *Atmos. Chem. Phys.*, 6, 1053–1073, doi:10.5194/acp-6-1053-2006, 2006.
1318
1319
1320 Zeng, G., Morgenstern, O., Shiona, H., Thomas, A. J., Querel, R. R., and Nichol, S. E.: Attribution
1321 of recent ozone changes in the Southern Hemisphere mid-latitudes using statistical analysis and
1322 chemistry-climate model simulations, *Atmos. Chem. Phys.* 17, 10495-10513, 2017.
1323
1324 Zhang, L., Jacob, D. J., Bowman, K. W., Logan, J. A., Turquety, S., Hudman, R. C., Li, Q., Beer,
1325 R., Worden, H. M., Worden, J. R., Rinsland, C. P., Kulawik, S. S., Lampel, M. C., Shephard, M.
1326 W., Fisher, B. M., Eldering, A., and Avery, M. A.: Ozone-CO correlations determined by the TES
1327 satellite instrument in continental outflow regions, *Geophys. Res. Lett.*, 33, L18804,
1328 doi:10.1029/2006GL026399, 2006.
1329
1330 Zhang, L., Jacob, D. J., Boersma, K. F., Jaffe, D. A., Olson, J. R., Bowman, K. W., Worden, J. R.,
1331 Thompson, A. M., Avery, M. A., Cohen, R. C., Dibb, J. E., Flock, F. M., Fuelberg, H. E., Huey,
1332 L. G., McMillan, W. W., Singh, H. B., and Weinheimer, A. J.: Transpacific transport of ozone
1333 pollution and the effect of recent Asian emission increases on air quality in North America: an
1334 integrated analysis using satellite, aircraft, ozonesonde, and surface observations, *Atmos. Chem.*
1335 *Phys.*, 8, 6117–6136, doi:10.5194/acp-8-6117-2008, 2008.
1336
1337 Zhang, L., Li, Q. B., Murray, L. T., Luo, M., Liu, H. and co-authors: A tropospheric ozone
1338 maximum over the equatorial Southern Indian Ocean. *Atmos. Chem. Phys.* 12, 4279-4296, 2012.
1339
1340 Zhang, Y., O. R. Cooper, A. Gaudel, A. M. Thompson, P. Nédélec, S.-Y. Ogino and J. J. West
1341 (2016), Tropospheric ozone change from 1980 to 2010 dominated by equatorward redistribution
1342 of emissions, *Nature Geoscience*, doi: 10.1038/NGEO2827, 2016.
1343
1344 Zhao, B., Wang, S. X., Liu, H., Xu, J. Y., Fu, K., Klimont, Z., Hao, J. M., He, K. B., Cofala, J.,
1345 and Amann, M.: NO_x emissions in China: historical trends and future perspectives, *Atmos. Chem.*
1346 *Phys.*, 13, 9869-9897, doi:10.5194/acp-13-9869-2013, 2013.
1347
1348 Ziemke, J. R., A.R. Douglass, L.D. Oman, S.E. Strahan, and B.N. Duncan: Tropospheric ozone
1349 variability in the tropics from ENSO to MJO and shorter timescales, *Atmos. Chem. Phys.*, 15,
1350 8037–8049, 2015.